The deep composition of Uranus and Neptune from in situ exploration and thermochemical modeling

Thibault Cavalié, Olivia Venot, Yamila Miguel, Leigh N. Fletcher, Peter Wurz, Olivier Mousis, Roda Bounaceur, Vincent Hue, Jérémy Leconte, Michel Dobrijevic

The deep composition of Uranus and Neptune from in situ exploration and thermochemical modeling

Thibault Cavalié · **Olivia Venot** · **Yamila Miguel** ·
Leigh N. Fletcher · **Peter Wurz** · **Olivier Mousis** ·
Roda Bounaceur · **Vincent Hue** · **Jérémy Leconte** ·
Michel Dobrijevic

Thibault Cavalié
Laboratoire d'Astrophysique de Bordeaux, Univ. Bordeaux, CNRS
B18N, allée Geoffroy Saint-Hilaire, 33615 Pessac, France
LESIA, Observatoire de Paris, PSL Research University, CNRS, Sorbonne Universités, UPMC Univ. Paris
06, Univ. Paris Diderot, Sorbonne Paris Cité
F-92195 Meudon, France
Tel.: +33-540003271
E-mail: thibault.cavalie@u-bordeaux.fr

Olivia Venot
Laboratoire Interuniversitaire des Systèmes Atmosphériques (LISA)
UMR CNRS 7583, Université Paris-Est-Créteil, Université de Paris, Institut Pierre Simon Laplace, Créteil,
France

Yamila Miguel
Leiden Observatory, University of Leiden
Niels Bohrweg 2, 2333CA Leiden, The Netherlands

Leigh Fletcher
School of Physics and Astronomy, University of Leicester
University Road, Leicester, LE1 7RH, UK

Peter Wurz
Universität Bern, Physikalisches Institut, Space Science and Planetology
Bern, Switzerland

Olivier Mousis
Aix Marseille Universit, CNRS, CNES, LAM
Marseille, France

Roda Bounaceur
Laboratoire Réactions et Génie des Procédés, LRGP UMP 7274 CNRS, Université de Lorraine
1 rue Grandville, BP 20401, F-54001 Nancy, France

Vincent Hue
Southwest Research Institute
San Antonio, Texas, USA

Jérémy Leconte
Laboratoire d'astrophysique de Bordeaux, Univ. Bordeaux, CNRS
B18N, allée Geoffroy Saint-Hilaire, 33615 Pessac, France

Michel Dobrijevic

Abstract The distant ice giants of the Solar System, Uranus and Neptune, have only been visited by one space mission, Voyager 2. The current knowledge on their composition remains very limited despite some recent advances. A better characterization of their composition is however essential to constrain their formation and evolution, as a significant fraction of their mass is made of heavy elements, contrary to the gas giants Jupiter and Saturn. An in situ probe like Galileo would provide us with invaluable direct ground-truth composition measurements. However, some of the condensibles will remain out of the grasp of a shallow probe. While additional constraints could be obtained from a complementary orbiter, thermochemistry and diffusion modeling can further help us to increase the science return of an in situ probe.

Keywords Uranus · Neptune · Ice Giants · Thermochemistry · Formation · Evolution

1 Introduction

In the early days of planetary sciences and space exploration, Uranus and Neptune seemed to be very much alike. They share relatively similar masses, radii and color, for example, suggesting these planets could be twins from their formation to their current state. However, even if these distant planets have only been visited once by a spacecraft, data acquired during the Voyager 2 flybys and more recently from ground-based and space-based facilities demonstrate that they are quite different. Their density differ by as much as 30%, Uranus is almost in equilibrium with incoming solar radiation while Neptune emits more than it receives (Pearl et al., 1990; Pearl and Conrath, 1991). Moreover, Uranus has a high obliquity causing an extreme seasonal forcing while Neptune's obliquity (and thus seasonal cycle) is probably more comparable to Saturn's one (Moses et al., 2018). Improved gravity field, shape and rotation rate data now seem to point to different internal structures and thermal evolution (Nettelmann et al., 2013, 2016; Helled et al., 2020).

As pointed out in e.g. Guillot (2005), Guillot et al. (2019), Atreya et al. (2020), Mousis et al. (2020), constraining the deep elemental and isotopic composition of the ice giants is one of the keys to better understand their formation and evolution. Unfortunately, and despite some recent progress (Sromovsky and Fry, 2008; Karkoschka and Tomasko, 2011; Irwin et al., 2018, 2019b; Tollefson et al., 2019a), deep abundance measurements in the ice giants remain scarce. The Galileo probe composition measurements in Jupiter's troposphere (von Zahn et al., 1998; Niemann et al., 1998; Mahaffy et al., 2000; Atreya et al., 1999; Wong et al., 2004) have triggered a tremendous amount of studies on the planet's formation (e.g. Owen et al., 1999; Gautier et al., 2001; Lodders, 2004; Guillot and Hueso, 2006; Mousis et al., 2012, 2019), now favouring the core accretion scenario for these planets (Pollack et al., 1996; Hubickyj et al., 2005) over the disk instability scenario (Boss, 1997, 2002). The formation and evolution of Uranus and Neptune, on the other hand, remains one of the most outstanding open question. Contemplating these major breakthroughs enabled by the Galileo probe measurements, now complemented by Juno observations (e.g. Bolton et al., 2017; Li et al., 2017, 2020; Kaspi et al., 2018), it seems obvious that the next great leap in understanding the formation and evolution of the Solar System will result from sending orbiters and probes to the ice giants. In addition, the expected advances in this field will undoubtedly have significant repercussions on our understanding of exoplanet formation

Laboratoire d'astrophysique de Bordeaux, Univ. Bordeaux, CNRS
B18N, allée Geoffroy Saint-Hilaire, 33615 Pessac, France

and evolution, since a significant fraction of the currently detected exoplanets are in the Neptune size-class[1].

Orbiter and probe missions to the ice giants that are currently under consideration (Mousis et al., 2018; Simon et al., 2018, 2020) will provide us with invaluable measurements in many fields, including bulk composition. In Section 2 of this paper, we will review the current knowledge of ice giants composition, with a comparison to gas giants, and the foreseeable prospects offered by ground-based and space-based observatories in the next decade. We will then show in Section 3 how thermochemical and diffusion modeling can help us further constrain the deep composition of ice giants in the absence of in situ composition measurements, and what the critical parameters of such models are. This will lead us to present in Section 4 the increased science return a descent probe making abundance measurements with a mass spectrometer in Uranus and/or Neptune would have if its results would be coupled to further thermochemical modeling, and to complementary remote sensing observations of the probe entry site for context, as well as the requirements on the instrument that such measurement/model coupling result in. Finally, we will review in Section 5 how deep composition measurements constrain interior and planetary formation models.

2 The composition of ice giants

Thermochemical models attempt to provide fits to the observed composition of a planetary atmosphere, by assuming a temperature profile, a deep mixing profile, and a set of chemical reactions. The bulk composition can only be measured in situ. The abundances measured by probes like Galileo are expected to be representative of the elemental composition at any location on the planet, especially for noble gases. The only known exception for Galileo is H_2O, because the probe descended into a hotspot (Orton et al., 1998). In addition to in situ measurements, remote sensing techniques can provide hints on the deep composition of giant planets, but they generally provide us with lower limits for condensible species and uncertainties are generally too large to be constraining for formation models. In some cases however, remote sensing can probe deeper than a shallow probe and could give better limits on the deep volatile composition. While the ultraviolet and mid-infrared can mostly reveal the stratospheric abundances of hydrocarbons, other wavelength ranges can be used to obtain more useful observations for the deep chemical abundance. For example, methane and hydrogen sulfide (H_2S) can be derived in the troposphere from the near-infrared reflectivity and, potentially, from remote sensing in the (sub)millimeter range, along with CO. Helium can be estimated from the far-infrared collision-induced continuum. These tropospheric species, which are largely pressure broadened, give us the strongest constraints on the deep composition.

In this Section, we will present the current knowledge on the upper tropospheric composition of the ice giants and a comparison with gas giants. We will conclude with the perspectives offered by current and future observatories that could be used prior to an ice giant probe arrival to derive the composition of these planets.

2.1 Observed elemental composition

The elemental abundances reviewed hereafter are summarized in Table 1 and compared to the solar and protosolar values. The present-day solar elemental abundances used in this

---

[1] https://exoplanets.nasa.gov/, http://exoplanet.eu

Table 1 Elemental abundances in the protosun and in giant planets.

Z	Element	Protosun (dex)	Jupiter/ Protosun	Saturn/ Protosun	Uranus/ Protosun	Neptune/ Protosun
2	He[a]	(10.99±0.01)	0.80±0.02	0.69±0.19	0.92±0.20	0.90±0.17
6	C[b,c]	(8.49±0.02)	3.85±0.95	8.58±0.37	80±20	80±20
7	N[d]	(7.88±0.05)	4.38±1.69	3.76±0.44	see text	see text
8	O[e]	(8.74±0.03)	>0.45±0.15			
10	Ne[f]	(7.98±0.10)	0.13±0.02			
15	P[g]	(5.46±0.03)	3.74±0.24	12.8±0.9		
16	S[h]	(7.17±0.03)	3.01±0.72	∼9	see text	see text
18	Ar[i]	(6.40±0.13)	3.23±0.65			
32	Ge[j]	(3.70±0.07)	0.058±0.008	0.046±0.046		
33	As[k]	(2.37±0.04)	2.35±0.15	7.38±2.49		
36	Kr[l]	(3.30±0.06)	2.33±0.44			
54	Xe[m]	(2.29±0.06)	2.28±0.46			

[a] Grevesse et al. (2010) for the protosun, von Zahn et al. (1998) and Niemann et al. (1998) or Jupiter, Conrath and Gautier (2000) for Saturn, Conrath et al. (1987) for Uranus and Conrath et al. (1993) for Neptune.

[b] Amarsi et al. (2019) for the protosun, Wong et al. (2004) for Jupiter, Fletcher et al. (2009a) for Saturn, Sromovsky and Fry (2008) for Uranus and Karkoschka and Tomasko (2011) and Irwin et al. (2019a) for Neptune (at the equator for Uranus and Neptune).

[c] As the CH_4 equatorial abundance is non negligible compared to He below its condensation level in both planets, it is accounted for when computing the H_2 mole fraction.

[d] Grevesse et al. (2010) for the protosun, Wong et al. (2004) for Jupiter, Fletcher et al. (2011) at the equator for Saturn. The recent Juno microwave measurement of Li et al. (2017) results in N/H=(2.76±0.30) times protosolar. For Uranus and Neptune, N/H is computed from S/H as an upper limit such that S/N>5×solar Irwin et al. (2018, 2019b).

[e] Amarsi et al. (2018) for the protosun, lower limit from Wong et al. (2004) for Jupiter.

[f] Scott et al. (2015) for the protosun, Mahaffy et al. (2000) for Jupiter.

[g] Scott et al. (2015) for the protosun, Fletcher et al. (2009a) for Jupiter and Saturn.

[h] Scott et al. (2015) for the protosun, Wong et al. (2004) for Jupiter, estimate from Briggs and Sackett (1989) for Saturn.

[i] Scott et al. (2015) for the protosun, Mahaffy et al. (2000) at the equator for Jupiter.

[j] Grevesse et al. (2015) for the protosun, Giles et al. (2017) for Jupiter, Noll and Larson (1991) for Saturn.

[k] Lodders (2010) for the protosun, Giles et al. (2017) for Jupiter, Noll and Larson (1991) for Saturn.

[l] Grevesse et al. (2015) for the protosun, Mahaffy et al. (2000) for Jupiter.

[m] Grevesse et al. (2015) for the protosun, Mahaffy et al. (2000) for Jupiter.

paper are all taken from Grevesse et al. (2010, 2015), Scott et al. (2015), Amarsi and Asplund (2017) and Amarsi et al. (2018, 2019), except for germanium and arsenic (Lodders, 2010). The protosolar elemental abundances are derived from the solar abundances following Grevesse et al. (2010).

The isotopic ratios are also very valuable in that they tell us the main reservoirs for the various elements. Isotopic measurements in hydrogen, noble gases, nitrogen, carbon, oxygen, etc. (e.g. Lellouch et al., 2001; Feuchtgruber et al., 2013; Mahaffy et al., 2000; Fouchet et al., 2000a; Fletcher et al., 2014) are therefore key in constraining protoplanetary disk physico-chemical conditions and planet formation models (e.g. Hersant et al., 2001; Owen and Encrenaz, 2003; Mousis et al., 2014b). However, isotopes have not yet been accounted for in thermochemical models. Recent progress in Titan photochemistry modeling (Dobrijevic et al., 2016) will enable that in the future. They are presented in more details in Atreya et al. (2020) and Mousis et al. (2020) and will not be discussed further in this paper.

2.1.1 Helium and noble gases

Voyager 2 provided the first measurement of the helium abundance of the giant planets from infrared spectroscopy and radio occultation experiments (Gautier et al., 1981; Conrath et al., 1984, 1987, 1991).

In Jupiter, the Galileo probe refined the measurement to an helium-to-hydrogen ratio (He/H) of $(7.85\pm0.16)\times10^{-2}$ (Niemann et al., 1998; von Zahn et al., 1998). In Saturn, the initial He/H of Conrath et al. (1984) was revised to a higher value of $(6.75\pm1.25)\times10^{-2}$ by Conrath and Gautier (2000). The He/H in Saturn remains uncertain and several attempts have been made recently to make new measurements. Using Cassini instrumentation, Koskinen and Guerlet (2018) and Waite et al. (2018) derived an He/H of $(5.5\pm1.0)\times10^{-2}$ and $\sim8\times10^{-2}$, respectively. Helium is therefore subsolar in both gas giant upper tropospheres, and this can be explained by the formation of helium droplets in metallic hydrogen (Wilson and Militzer, 2010).

The initial results at Uranus and Neptune helium indicated mole fractions of 0.152 ± 0.033 (Conrath et al., 1987) and 0.190 ± 0.032 (Conrath et al., 1991), respectively. Accounting for an N_2 mole fraction of 0.003 in Neptune's atmosphere enabled Conrath et al. (1993) to revise their results to 0.15 for Neptune, bringing it in better agreement with the Uranus value. Later Infrared Space Observatory (ISO) observations by Burgdorf et al. (2003) seem to confirm and further refine the Neptune helium abundance to $0.149^{+0.017}_{-0.022}$. The He/H in Uranus and Neptune would thus seem to be slightly subsolar with abundances of $(8.88\pm2.00)\times10^{-2}$ and $(8.96\pm1.46)\times10^{-2}$, respectively. However, the error bars remain too large (from subsolar to marginally supersolar) to constrain interior models accurately (Guillot, 2005; Helled et al., 2011; Helled and Guillot, 2018; Helled et al., 2020; Nettelmann et al., 2013). Remote sensing can only provide tentative results and it is clear that only in situ measurements can provide us with a measurement accurate enough to constrain formation and evolution models. The goal of a probe is to reach an accuracy of 2% (Mousis et al., 2018), similar to Galileo.

Noble gases beyond helium have only been measured in Jupiter by the Galileo probe. Argon, Xenon and Krypton were all found enriched by a factor of 2-4 with respect to the protosolar value. Only neon is found subsolar, because of dissolution in liquid helium deep in the atmosphere of Jupiter (Roulston and Stevenson, 1995; Wilson and Militzer, 2010).

2.1.2 Carbon

Methane is the most abundant species after helium in all giant planets, and it is their main carbon reservoir.

In Jupiter, Galileo measured C/H=$(1.19\pm0.29)\times10^{-3}$ (Wong et al., 2004). At Saturn, Fletcher et al. (2009b) used Cassini to constrain C/H to $(2.65\pm0.10)\times10^{-3}$.

In the ice giants, methane condenses at ~1 bar and must be measured below this level. Its mole fraction was initially measured to about 0.02 (Lindal et al., 1987; Lindal, 1992; Baines et al., 1995) in both ice giants, i.e. more than an order of magnitude above its stratospheric abundance (Lellouch et al., 2015). More recent observations have, however, shown that the picture is more complicated than initially thought. Karkoschka and Tomasko (2009, 2011), Sromovsky and Fry (2008), Sromovsky et al. (2011, 2014), and Irwin et al. (2019a) have used near-IR scans that sample both an H_2-collision induced opacity and a methane opacity to separate the effects of clouds and methane. From these spatially-resolved observations, they have shown that methane is more abundant at low latitudes than at the high latitudes sampled by the earlier observations. The equatorial mole fraction of methane is

0.04±0.01 decreasing towards the poles in the upper troposphere possibly because of tropospheric circulation (Fletcher et al., 2020a). This point will be briefly addressed in Section 3.5.1. In any case, methane is being measured at the CH_4-ice condensation point, and there is a possibility that there is additional internal stratification, as seen with jovian ammonia that is not well-mixed beneath the expected cloud-condensation level (e.g. Li et al., 2017). The current measurements must therefore be seen as lower limits on the deep C/H in ice giants.

2.1.3 Sulphur and nitrogen

Sulphur and nitrogen should be mainly borne by H_2S and ammonia (NH_3) in the reducing part of the atmospheres of the giant planets, even if the $^{15}N/^{14}N$ isotopic ratio in Jupiter and Saturn suggests nitrogen may have originally been delivered from N_2 (Fouchet et al., 2000a; Fletcher et al., 2014; Mousis et al., 2014b). Both nitrogen and sulphur should be enriched over the protosolar value.

Both have been observed in Jupiter by Galileo with N/H=(3.32±1.27)×10^{-4} and S/H=(4.45±1.05)×10^{-5} (Wong et al., 2004). More recent microwave mapping observations of Juno indicate that NH_3 is not well-mixed in the jovian upper troposphere, at least above the 50-60 bar level (Bolton et al., 2017; Li et al., 2017), raising the question whether the Galileo measurement is representative of the nitrogen deep abundance. They find a deep NH_3 mole fraction of 362±33 ppm, i.e. N/H=(2.09±0.20)×10^{-3} only marginally consistent with the Galileo measurement done at 6.5° north. In Saturn, Fletcher et al. (2011) found N/H=2.85×10^{-4} at the equator from Cassini/VIMS, confirmed by Cassini/RADAR observations of Janssen et al. (2013) and Laraia et al. (2013). However, its deep value remains quite uncertain due to meridional variability, similarly to the Jupiter case (Li et al., 2017). The detection of H_2S in Saturn remains uncertain (Briggs and Sackett, 1989).

In the ice giants, H_2S and NH_3 remained undetected for a long time despite repeated efforts. The reason is that both species are thought to form a cloud of ammonium hydrosulfide (NH_4SH) at around 30-50 bars from the $NH_3(g) + H_2S(g) \rightarrow NH_4SH(s)$, only leaving traces of the most abundant species among the two up to their own condensation level (DeBoer and Steffes, 1994). The most abundant of the two would then condense in another cloud, at pressures between 5 and 10 bars. de Pater and Richmond (1989) and de Pater et al. (1989) found that NH_3 had to be ∼0.1-0.001 times solar in the probed part of the atmosphere to match their microwave spectra of the two planets. To explain this depletion, de Pater et al. (1991) tentatively proposed an abundance of H_2S 10-30 times solar and an S/N at least 5 times solar in Uranus. Similar conclusion were reached for Neptune by DeBoer and Steffes (1994, 1996). However, these abundances must all be understood as lower limits since none of these observations probed below the NH_4SH cloud base. Using near-infrared observations with the Gemini North telescope, Irwin et al. (2018) detected H_2S above the main cloud deck in Uranus, indicating that sulphur is more abundant than nitrogen and placing a lower limit on their ratio, with S/N > 4.4-5.0 times the solar value (in agreement with de Pater et al. 1991). Using a similar technique, Irwin et al. (2019b) derived a lower limit on H_2S in Neptune. Complementary broadband spectra obtained with the VLA and ALMA enabled Tollefson et al. (2019a,b) to tentatively constrain S in Neptune to be 30 times protosolar and N to be protosolar.

2.1.4 Oxygen

Water, the main oxygen-bearing species in a giant planet interior, played a crucial role when giant planets formed. Water ice at the time of planetesimal formation provided a significant mass reservoir to build the planetary cores beyond the snowline, and the C/O ratio is a good diagnostic of the planet formation location (Ali-Dib et al., 2014; Mousis et al., 2012, 2014b; Öberg et al., 2011; Öberg and Bergin, 2016).

In addition, these ices played a fundamental role in that they trapped the other heavy elements. Depending on the pressure and temperature conditions at which the ices condensed, the heavy elements were either trapped on amorphous ices or in clathrates (Bar-Nun et al., 1988; Owen et al., 1999; Lunine and Stevenson, 1985; Gautier et al., 2001; Gautier and Hersant, 2005; Mousis et al., 2006). If ices condensed in amorphous form, then the oxygen enrichment should be similar to the enrichment of other heavy element (Owen and Encrenaz, 2003, 2006). On the other hand, the clathrate scenario requires a radically different oxygen abundance, i.e., ∼4 times more, to trap the heavy elements (Mousis et al., 2014b, 2018). This is why constraining the deep oxygen abundance is so important to understand giant planet formation.

The Galileo probe entered a 5-μm hotspot and failed to reach the levels where water is uniformly mixed in Jupiter (Atreya et al., 2003; Wong et al., 2004). Juno is currently attempting to make this measurement from microwave radiometry during low-altitude perijove passes (Matousek, 2007; Bolton et al., 2017), now that the NH_3 distribution is established (Li et al., 2017). The first result obtained in the equatorial zone, where NH_3 is well-mixed up to its condensation level, indicates an O/H=$2.7^{+2.4}_{-1.7}$ times protosolar (Li et al., 2020). This result is key to better understanding the formation of Jupiter (Helled and Lunine, 2014), but will require additional measurements at other latitudes to assess whether this is the bulk abundance.

In the other giants, the tropospheric temperatures are colder than in Jupiter, making water condensation happen deeper. While reaching the well-mixed layers in Saturn will be at the limit of the capabilities of recently proposed probe (Mousis et al., 2014a, 2016; Atkinson et al., 2016, 2018), direct in situ measurement will remain highly improbable in the ice giants because water condenses at a pressure ranging between ∼200 and ∼1000 bar, depending on the adopted temperature extrapolation model (Atreya and Wong, 2005; Leconte et al., 2017). Complementary measurements taken by a remote sensing instrumentation suite on future ice giant orbiters (e.g. Arridge et al., 2014) will therefore be needed for additional context and constraints.

In the meantime, indirect measurements are the only possibility to constrain the deep oxygen abundance in these planets. We will detail these techniques and recent progress in Section 3.

2.1.5 Phosphorus and other heavy elements

Phosphorus, mainly carried by phosphine (PH_3), was observed with Cassini by Fletcher et al. (2009a) and the P/H ratio is $(1.08\pm0.06)\times10^{-6}$ in Jupiter and $(3.70\pm0.23)\times10^{-6}$ in Saturn. However, it still remains undetected in the ice giants (Moreno et al., 2009; Teanby et al., 2019). It may result from the destruction of this species by H_2O thermochemistry at depth, provided that the deep oxygen abundance is high enough in both planets (Visscher and Fegley, 2005).

Other heavy-element-bearing species have been observed in Jupiter and Saturn, like GeH_4 and AsH_3 (Giles et al., 2017; Noll and Larson, 1991; Fletcher et al., 2011). As is

supersolar in Jupiter, like most other heavy elements, but Ge is subsolar. This probably results from deep thermochemistry as Ge atoms are partly transferred from GeH_4 to GeS around the GeH_4 quench level (Lodders and Fegley, 1994). A complication arises from the non uniform meridional abundances of these species. While GeH_4 and PH_3 peak at low latitudes and decreases poleward, as expected from models (Wang et al., 2015), AsH_3 is minimal at low latitudes and peaks at the poles (Grassi et al., 2019). Their deep abundance thus remains quite uncertain.

2.1.6 Summary

Most heavy element abundance measurements were made possible by sending an entry probe in Jupiter. This underlines the importance of sending such instrumentation to all giant planets in the Solar System to make comparable ground-truth measurements. If these were coupled to remote sensing from orbiting facilities, the direct measurement would help to break the degenerate effects of gaseous species on the planetary spectrum.

Besides the elements presented previously, Galileo enabled quantifying the abundances of noble gases such as neon, argon, krypton, and xenon (Mahaffy et al., 2000). All elements measured by the probe are 2-4 times solar (except oxygen for the reasons mentioned above). The Juno measurement of oxygen will complete this panorama, but preliminary results that pertain to Jupiter's equatorial zone are compatible with this picture (Li et al., 2020).

In Saturn, helium is subsolar probably because of helium rain, carbon and phosphorus are about 10 times solar, but nitrogen seems to be less enriched. The non uniformity of the meridional distribution of NH_3 (Fletcher et al., 2011), similarly to Jupiter (Bolton et al., 2017; Li et al., 2017), complicates the derivation of the deep nitrogen abundance. The lack of measurements for other heavy elements, especially noble gases which should be uniform with altitude and latitude, makes it difficult to constrain Saturn formation models (e.g. Hersant et al., 2008). Several probe proposals were developed in the recent years (Atkinson et al., 2016, 2018; Mousis et al., 2014a, 2016) but none was selected for flight so far.

In Uranus and Neptune, the scarcity of heavy element abundance measurements is even more dramatic than in Saturn, as only carbon and, to some extent, sulphur have been measured, though the measurements of these condensible species bear large error bars and might be lower limits. The nominal abundance of methane at 1-2 bars and at low latitudes in both planets results in a C/H of 0.04$\pm$0.01, i.e., about 80 times protosolar, as expected from models (Owen and Encrenaz, 2003; Hersant et al., 2004). Sulphur may be 20-30 times protosolar, slightly lower than predictions from those same models.

This summary stresses the need for planetary probes at Saturn, and even more so at the ice giants.

2.2 Perspectives on ice giant elemental composition determination ahead of the 2040s

If a probe-carrying mission is to be selected for Uranus and/or Neptune with a launch window in the 2029-2034 timeframe (Simon et al., 2020), such a mission will arrive in the 2040s. In this Section, we will attempt to list the progress on ice giant composition we can expect from existing and forthcoming ground-based and space-based observatories. In addition, these observations ahead of a mission arrival in the 2040s will enable temporal variation studies which will set the ground for the mission operations and help contextualize them further.

2.2.1 Radio

Radio wave observations probe the giant planet spectra where NH_3, H_2S and H_2O absorb. Single dish observations in the centimeter to decameter range remain difficult to calibrate accurately enough for the measurements to be constraining (Courtin et al., 2015). Interferometric observations of Saturn with LOFAR (Low Frequency Array, Röttgering 2003) have not yet detected Saturn's emission unambiguously because of the low planetary flux combined with the rapidly varying background sky emission (D. Gautier, private communication, 2015). The implementation of the Square Kilometer Array (SKA) may enable achieving these long wavelength measurements to better constrain the deep NH_3 and H_2O abundances in the giant planets in the 2030s.

In the centimeter wavelengths, the e-VLA (expanded Very Large Array) remains the best radio observatory to date. A project to improve the capabilities in terms of spatial resolution and sensitivity, named the ng-VLA (next generation VLA), may enable to improve on the constraints on deep N, S and O in the ice giants (de Pater et al., 2018). This project is aiming to start early science operations in the late 2020s and full science operations in the mid-2030s.

However, it remains to be seen whether radio measurements can probe deep enough and reach the well-mixed layers with the required accuracy. Juno has shown for NH_3 in Jupiter that reaching the well-mixed region requires probing at tens of bars (Bolton et al., 2017; Li et al., 2017). Interpreting the radio emission uniquely remains a challenge because it is hard to separate the broad spectral effects of temperature and the gaseous opacity.

2.2.2 Millimeter and submillimeter

ALMA (Atacama Large Millimeter/submillimeter Array) and NOEMA (NOrthern Extended Millimeter Array) are currently the most sensitive millimeter and submillimeter interferometers. Both will still be operating in the 2020s and 2030s.

Aggregating broadband observations of these arrays with ng-VLA observations will help to improve our understanding of spatial distribution of H_2S and NH_3 (see Tollefson et al. 2019b for results using the current capabilities of these observatories) and of upper tropospheric circulation (Fletcher et al., 2020a) in the ~1-50 bar pressure range. In addition, the determination of the meridional distribution of tropospheric CO in Uranus and Neptune from line spectroscopy will help to constrain further the deep oxygen abundance by coupling the observations to thermochemical modeling (see Section 3).

2.2.3 Near, mid- and far-infrared

In the near-IR, the techniques for separating the reflective aerosols from gaseous composition (specifically CH_4 and H_2S) have been established by ground-based observers using the largest astronomical facilities (e.g., Gemini, Keck, Very Large Telescope, etc.). These have demonstrated latitudinal variations of these volatiles, and provided lower limits on the potential bulk abundances of carbon and sulphur. Future near-infrared ground-based measurements with higher spatial resolutions (e.g., from the next generation of instrumentation on extremely large telescopes, such as the Extremely Large Telescope, Giant Magellan Telescope and Thirty Meter Telescope) might allow for further discrimination between aerosols and gaseous composition, but these may still be hampered by terrestrial atmospheric contamination. In the mid-infrared and far-infrared, measurements from ground- and airborne

facilities (e.g., Stratospheric Observatory for Infrared Astronomy) could continue to determine stratospheric composition and thermal structure, but this may not be of use for the determination of bulk planetary composition (with the exception of deuterium-to-hydrogen ratio measurements, if possible in the far-infrared).

In all of these cases, further progress could be made by being above the complicating effects of the terrestrial atmosphere. The James Webb Space Telescope (JWST, Gardner et al. 2006) carries instruments spanning the 1-30 micron range at exquisite spectral resolution and sensitivity that surpasses anything from the ground (Norwood et al., 2016a,b). In the mid-infrared, the MIRI instrument will place new upper limits on the PH_3 and NH_3 content using bands near 5 and 10 microns that have never been observed before. MIRI will also constrain the collision-induced continuum in the far-infrared, which may enable separation of temperature, para-H2 and helium, via the same techniques as used on Voyager IRIS. MIRI will also provide our first spatially-resolved glimpses of the stratospheric temperatures and chemistry (Moses et al., 2018).

In the near-infrared, NIRSpec will enable more sensitive measurements of the H_2S and CH_4 abundances using the techniques honed on the ground. Furthermore, they will provide access to fluorescent regions between 3.0-4.5 microns, where CO and CO_2 fluoresce (Encrenaz et al., 2004; Fletcher et al., 2010). Along with sub-millimetre observations of CO, these provide another independent measurement of the CO abundance on the ice giants. In addition, the JWST instruments will further refine the D/H ratio in CH_4 (and potentially other species), as a further constraint on planetary formation.

At longer wavelengths in the far-infrared and sub-millimetre, the proposed Origins Space Telescope (OST, Leisawitz et al. 2018) and the SPace Infrared telescope for Cosmology and Astrophysics (SPICA, Roelfsema et al. 2018) will both offer sensitive observations of the spectrum, potentially allowing new constraints on the shape of the hydrogen-helium continuum, and on the isotopic ratios within hydrogen (from far-IR HD features). Depending on the final architecture of these missions, they may also provide new measurements of rotational lines of CO and CH_4. Even with these new and sensitive instruments, the ice giants will likely be unresolved, such that no spatial variability in these gases will be measured. For this, we have to be reliant on future orbital missions to the ice giants.
These future observations concern several species that can be further used to constrain the deep abundance of some key elements by combining these observations with thermochemical modeling. This is the subject of the next Section.

3 Thermochemical modeling of giant planet atmospheres

In this Section, we will first present the principle of inferring deep planet composition from thermochemical modeling. We will then review the models that dealt with giant planet thermochemistry through the quench level approximation and show the recent progress enabled by the development of more comprehensive thermochemical and diffusion models. Finally, we will detail the parameters these models rely on and what the prospects on improving their predictability is.

The deep hot troposphere of the giant planets is in thermochemical equilibrium. If applied to the upper troposphere and to the stratosphere, this equilibrium predicts extremely small abundances for many species that have nonetheless been detected (Prinn and Barshay, 1977; Fegley and Prinn, 1985, 1986; Fegley and Lodders, 1994), among which the methyl radical (CH_3 ; Bézard et al. 1998, 1999, Fouchet et al. 2018a), stable hydrocarbons (Gladstone and Yung, 1983; Fouchet et al., 2000b; Courtin et al., 1984; Orton et al.,

2014; Burgdorf et al., 2006; Meadows et al., 2008), phosphine (PH_3 ; Knacke et al., 1982; Bregman et al., 1975; Fletcher et al., 2009a, carbon monoxide (CO ; Beer, 1975; Bézard et al., 2002; Noll et al., 1986; Noll and Larson, 1991; Encrenaz et al., 2004; Marten et al., 1993, 2005), carbon dioxide (CO_2 ; Feuchtgruber et al. 1997, Burgdorf et al. 2006), hydrogen cyanide (HCN ; Lellouch et al. 1995, Bézard et al. 1997, Fouchet et al. 2018b, Marten et al. 1993), carbon sulfide (CS ; Lellouch et al. 1995; Moreno et al. 2017). These species are generally observed in the stratosphere. They are produced from CH_4 photochemistry (Moses et al., 2000a, 2005, 2018; Dobrijevic et al., 2010, 2011, 2020; Hue et al., 2015, 2016, 2018) or injected in the atmosphere from external sources (Feuchtgruber et al., 1997; Moses et al., 2000b; Ollivier et al., 2000), like interplanetary dust particles (Landgraf et al., 2002; Moses and Poppe, 2017), large comet impacts (Lellouch et al., 1995, 2005, 2006; Cavalié et al., 2008, 2010, 2012, 2013; Moreno et al., 2017), and icy rings and satellites (Connerney and Waite, 1984; Connerney, 1986; Prangé et al., 2006; Hartogh et al., 2011; Waite et al., 2018; Perry et al., 2018; Cavalié et al., 2019). However, others like CO and PH_3 are observed in the upper troposphere[2] with abundances that are tens of orders of magnitude above thermochemical equilibrium predictions. Their presence at these levels is caused by convective vertical mixing that quenches thermochemical equilibrium where the vertical transport timescale becomes shorter than the chemical timescale.

Thermochemical and diffusion modeling can then be a powerful tool to infer the deep elemental composition of the giant planets from disequilibrium species, especially when the main carrier of an element does not reach the observable levels. The disequilibrium species abundances is used to track back their abundance at their respective quench level to then tie them back to the main element-carrier abundance.

In this Section, we will present the modeling principle of thermochemistry to constrain deep composition and show how it has been applied in the past decades, first using the quench level approximation, and then using more comprehensive chemical models. We will detail the parameters that are fundamental in getting accurate simulations and the prospects regarding future improvements.

3.1 Principle

Oxygen is mainly carried by water, but water condenses in the troposphere of the giant planets. While its condensation level occurs at $\sim$10 bar in Jupiter, it occurs at pressure ranging from $\sim$200 to $\sim$1000 bars in both Uranus and Neptune, according to temperature extrapolation models (Leconte et al., 2017). Only microwaves can probe that deep (Janssen et al., 2005; de Pater et al., 2016), but limited calibration accuracy often prevents any direct constraint on the water abundance (de Pater and Richmond, 1989; de Pater et al., 1989; Courtin et al., 2015). The idea then lies in measuring the upper tropospheric abundance of CO, which does not condense in giant planet atmospheres and is in disequilibrium because of efficient vertical mixing, and to tie it back to the deep water abundance with a chemistry and diffusion model. As CO is chemically linked to water, thermochemical and diffusion models have been used with this species to constrain the deep oxygen abundance ever since it was first detected in Jupiter by Beer (1975).

Other carbon bearing species can, in principle, be used similarly to constrain the deep water, like ethane (C_2H_6) (Fegley and Lodders, 1994). Another example is phosphorus, which has been detected in PH_3 in Jupiter and Saturn, but neither in Uranus nor in Neptune

---

[2] CO can actually have an internal and an external component (Bézard et al., 2002; Lellouch et al., 2005).

(Moreno et al., 2009). This species can be destroyed by water if water is abundant enough. Its detection then results either from the relatively low water abundance or from its quenching at levels that are deeper than where it gets destroyed by water (Fegley and Lodders, 1994). On the other hand, its absence can help to put additional constraints on the deep water abundance (Visscher and Fegley, 2005).

We come back to the example of carbon monoxide and water, as it is the most studied case to date. In the deep hot tropospheres of giant planets, CO and H_2O are in thermochemical equilibrium through the reaction

$$H_2O + CH_4 = CO + 3H_2. \tag{1}$$

Rearranging the equilibrium constant of the above equation enables to express the CO mole fraction as follows:

$$y_{CO} = \frac{y_{CH_4} y_{H_2O}}{y_{H_2}^3 p^2} K_{eq} \tag{2}$$

where p is the total pressure and K_{eq} is the equilibrium constant of reaction (1). At higher and colder levels, the H_2O-CO equilibrium moves towards the reduced H_2O-CH_4 mixture and the conversion kinetics slows down. There is a level in the troposphere at which the temperature is low enough for the kinetics to become slower than the vertical mixing caused by convection. This is the level where the chemical lifetime of CO destruction τ_{chem} equals the vertical mixing timescale τ_{mix}. Thermochemistry is quenched and the CO mole fraction fixed for all levels above this quench level.

There are two techniques that have been used to find the abundances of CO and water at the quench level: the quench level approximation and comprehensive thermochemical and diffusion modeling. In both cases, presented below, the determination of convective mixing is crucial.

3.2 Estimating convective mixing strength

The magnitude of vertical mixing caused by convection is key in fixing the level at which thermochemistry is quenched, and in turn in fixing upper tropospheric abundances of disequilibrium species: the stronger the mixing, the deeper the quench level.

The vertical mixing timescale τ_{mix} is given by

$$\tau_{mix} = \frac{L^2}{K}, \tag{3}$$

where K the vertical mixing coefficient and L the length over which mixing occurs. The latter was taken as the atmospheric scale height H in early studies. Convective mixing can be estimated from free-convection and mixing-length theories (Stone, 1976; Gierasch and Conrath, 1985) and modeled in 1D models by means of an eddy mixing coefficient. The scaling relationship

$$K \simeq \left(\frac{F k_B}{\rho m c_p} \right)^{\frac{1}{3}} H, \tag{4}$$

where F is the internal heat flux of the planet, k_B is the Boltzmann constant, ρ is the atmospheric mass density, m is the atmospheric mean molecular mass, and c_p is the atmospheric specific heat at constant pressure, applies in the absence of rapid rotation and a strong magnetic field. It is therefore only an approximation for giant planets. These estimates show that tropospheric K is of the order of 10^8 $cm^2 \cdot s^{-1}$, with a factor of 10 uncertainty, in the giant

planets. Visscher et al. (2010) derived an altitude-latitude dependent expression for K for fast rotating planets. They showed that K decreased both with latitude and depth. The decrease with depth can however be neglected in thermochemical simulations because the variation is less than an order of magnitude between the top of the troposphere and the quench level. More recently, Wang et al. (2015) used rotating tank experiments to refine the scalings in the expression of K, and thus decrease the uncertainty on their estimation down to about 25%. They also predicted that K would be maximum at low latitudes and then decrease towards the high latitudes. They found that the decrease caused by depth and latitude was steeper for Saturn than for Jupiter. We illustrate the application of their prescription to Uranus and Neptune in Fig. 1. It essentially shows that disequilibrium species like CO, GeH_4 and PH_3 that are quenched where their abundance decreases with height should be more abundant in the upper troposphere at low latitudes. On the contrary, disequilibrium species like AsH_3 that are quenched where their abundance increases with height (Fegley and Lodders, 1994) should be more abundant at high latitude in the upper troposphere. This seems to be qualitatively in line with Juno/JIRAM observations of Jupiter (Grassi et al., 2019).

3.3 Quench level approximation

By decomposing the thermochemical equilibrium reaction (Equation 1) into the series of reactions that lead H_2O to be converted into CO (and vice versa), one can then try and identify the reaction which has the slowest kinetics, i.e. the rate-limiting reaction. The estimation of the rate-limiting reaction kinetics constrains the kinetics of the whole conversion scheme. By equating τ_{chem} and τ_{mix}, it is then possible to derive the temperature at the quench level. Assuming a pressure-temperature relationship (e.g., dry or wet adiabat), it is then possible to compute p in Equation 2. The measured upper tropospheric mole fractions of CO and CH_4, which are the same as the one at the quench level, can eventually be used to solve the system and derive the deep value of y_{H_2O}.

(Prinn and Barshay, 1977) first identified this rate-limiting reaction to be $H_2 + CH_2O \rightleftharpoons CH_3 + OH$. By assuming a solar composition, they constrained vertical mixing to reproduce the CO detection of Beer (1975), thus using thermochemistry the other way around. Later work by Fegley and Prinn (1985, 1988) and Fegley and Lodders (1994) further explored the deep composition of Jupiter and Saturn. Bézard et al. (2002) performed high spectral resolution observations in the 5μm window in the North Equatorial Belt of Jupiter to refine the planet's CO upper tropospheric abundance to 1.0 ± 0.2 ppb. They applied the less ambitious kinetic scheme of Yung et al. (1988) for the CO-CH_4 conversion, in which the rate-limiting reaction is $H + H_2CO + M \rightleftharpoons CH_3O + M$. They also used the new method of Smith (1998) to estimate the vertical scale for diffusion (in replacement of H in Equation 3). They derived a jovian deep oxygen abundance of 0.2 to 9 times the solar value.

The quench level approximation was later used in several studies (Visscher and Fegley, 2005; Cavalié et al., 2009; Luszcz-Cook and de Pater, 2013) following the detections of CO in Saturn and Neptune by Noll et al. (1986) and Marten et al. (1993) to try and constrain the deep oxygen abundance in these planets.

3.4 1D kinetic and diffusion models

Another approach used to constrain the deep water abundance consists in using detailed kinetic and diffusion models that are able to reproduce accurately the chemical composition
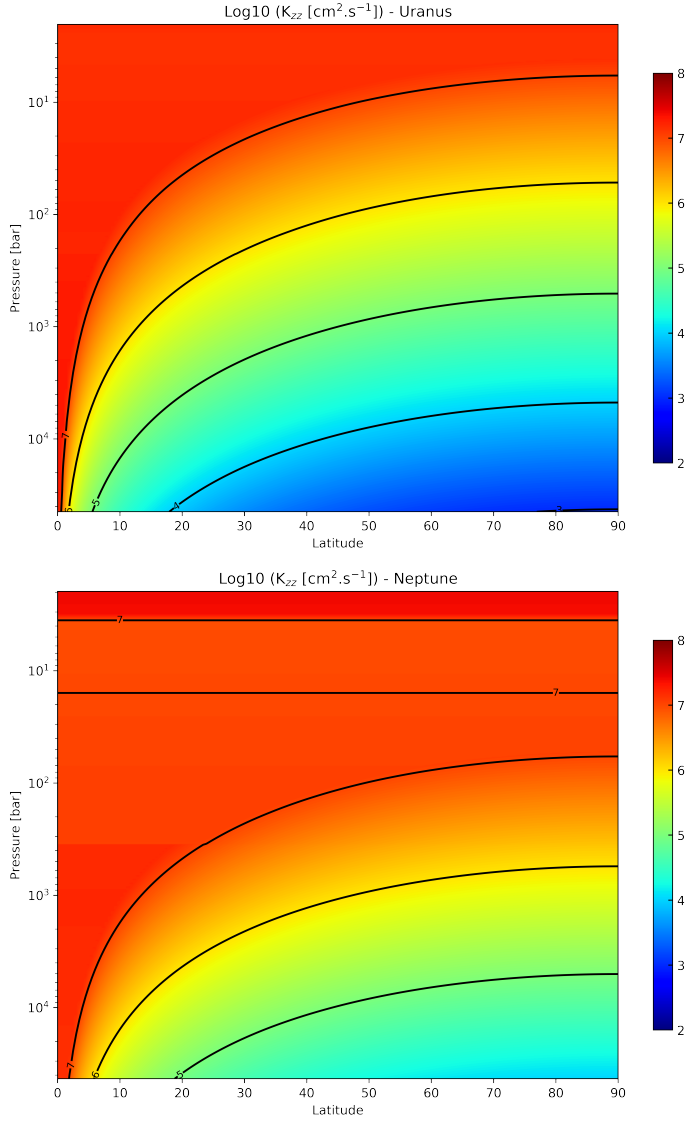
Fig. 1 Vertical mixing in the tropospheres of Uranus (top) and Neptune (bottom) as a function of pressure and latitude, using the prescription of Wang et al. (2015) and the temperature and abundance profiles of Venot et al. (2020).

of hot atmospheric regions. The development of such models has been motivated by the discovery of hot giant exoplanets and the interpretation of their infrared spectra. Despite the high temperatures prevailing in their atmospheres, the regions probed by spectroscopic observations are not at thermochemical equilibrium. Disequilibrium processes are important and disturb the atmospheric composition. Thus, thermo-photochemical models have been developed specifically for the study of these peculiar atmospheres in which thermochemical

Table 2 Deep oxygen abundance in giant planet deep atmospheres.

	CO mole fraction (upper troposphere)	Deep O/H ($\times$ protosun)	Reference
Jupiter	(1.0 ± 0.2) ppb	0.26-6.3	Bézard et al. (2002), Visscher et al. (2010)
Saturn	$\sim$1 ppb	10-70	Fouchet et al. (2017), Wang et al. (2016)
Uranus	$<$2.1 ppb	$<$45	Teanby and Irwin (2013), Venot et al. (2020)
Neptune	(0.20 ± 0.05) ppm	250	Luszcz-Cook and de Pater (2013), Moreno et al. (2011), Venot et al. (2020)

[a] Oxygen abundances have been rescaled using the protosolar abundances of Table 1.

equilibrium, mixing and photochemistry are at play (e.g. Moses et al., 2011; Visscher and Moses, 2011; Venot et al., 2012; Drummond et al., 2016; Tsai et al., 2017).

These models enable an accurate computation of the vertical profiles in the key pressure range where quenching occurs. They have been used for each solar system giant planet (Visscher et al., 2010; Wang et al., 2016; Cavalié et al., 2014, 2017) to further constrain their deep oxygen abundances. Table 2 summarizes the current status of model results regarding deep oxygen abundance in all giant planets.

3.5 Perspectives prior to an ice giant probe mission

Thermochemical and diffusion models, like quench level models, still have to rely on several parameters that have to be assumed, i.e. the vertical mixing and the pressure-temperature profile. The main differences between their results then boil down to the differences in their chemical schemes. In this Section, we will review the progress we anticipate prior to the arrival of an ice giant probe in the 2040s regarding the determination of these input parameters.

3.5.1 Vertical mixing

Visscher et al. (2010) showed that vertical mixing caused by convection in giant planet tropospheres depends on latitude and altitude, because of the planet rotation. Wang et al. (2015) further refined these calculations and concluded that the magnitude of this vertical mixing would decrease with latitude and depth. Its maximum is anticipated at the low latitudes. This means that the deepest quench levels, and therefore the highest abundances for species like CO and GeH_4, are expected to be observable at these same low latitudes. This is confirmed by recent Juno observations at Jupiter for GeH_4 (Grassi et al., 2019).

However, the picture in giant planet upper tropospheres seems to be more complex than initially thought. In Jupiter, the abundance of NH_3 is far from the idealized well-mixed picture in the 1-50 bar range, with only a narrow band slightly north of the equator being uniformly mixed up to the NH_3 cloud (Bolton et al., 2017; Li et al., 2017; de Pater et al., 2019). Guillot et al. (2019) proposed that this distribution is likely caused by the formation of NH_3-H_2O mesh balls in convective storms. Such an equatorial plume had already been identified by Fletcher et al. (2009a) in Jupiter's and Saturn's PH_3 distributions. In Neptune, Tollefson et al. (2019a,b) showed that condensibles like H_2S and NH_3 were subject to tropospheric circulation and/or meteorology and that the circulation pattern extends down to the $\sim$30 bar level.

Disk-resolved tropospheric observations with facilities like e.g., ALMA, e-VLA and JWST, and 3D general circulation model (GCM) are therefore required to better understand upper tropospheric circulation and chemistry (Fletcher et al., 2020b,a). Venot et al. (2019, 2020) have proposed a reduced chemical scheme from their more complete 1D thermochemical model in view of their implementation in more complex 3D GCMs. Nailing down the latitude range where vertical mixing is most efficient in transporting disequilibrium species up to observable levels will be key in setting the entry latitude to target in priority with a shallow probe to increase its chances to access the well-mixed region of the explored atmosphere.

3.5.2 Temperature profile

One of the main unknown in giant planet tropospheres is the temperature-pressure field. It bears implication on circulation, kinetics, condensation layers, vertical mixing, etc. Except the Galileo probe measurements, which probed Jupiter down to the 22 bar level (Seiff et al., 1998), there is no such deep temperature measurement in any other giant planet. The fact that Galileo entered a 5μm hot spot further questions the representativeness of the measurements. In the other giants, there is a large uncertainty beneath the 2 bar level, which is the deepest level probed by occultation with Voyager 2 (Lindal et al., 1985, 1987, 1990; Lindal, 1992). Moreover, latitudinal variability remains unconstrained, even if the observed tropospheric distributions of several condensibles are hints of such variability (Sromovsky and Fry, 2008; Karkoschka and Tomasko, 2011; Irwin et al., 2019a; Tollefson et al., 2019a; Molter et al., 2019).

Extrapolation to higher pressures are required for thermochemical computations and a dry or a wet adiabat has often been used (Luszcz-Cook and de Pater, 2013). However, Guillot (1995) first showed that Uranus and Neptune are in a situation where mean molecular weight gradients could inhibit convection at the condensation level of CH_4 and produce in a steep increase of the temperature. Later, Leconte et al. (2017) demonstrated that the effect of convection inhibition would be even more dramatic deeper, at the H_2O condensation level. The resulting profile would then be a "3-layer profile", starting from a wet adiabat in the uppermost levels, a radiative layer where the water vapor mixing ratio is between a fixed critical value and its maximum internal value, and a dry adiabat deeper down. The range of possible temperature profiles in Uranus and Neptune, between the wet adiabat (the coldest) and the convection inhibited one (the warmest), are shown in Fig. 2. Cavalié et al. (2017) showed that the implications on the deep composition as derived from thermochemical modeling are significant. Therefore, any improvement in our knowledge of the tropospheric temperature is regarded as highly valuable.

3.5.3 Chemical scheme

The chemical scheme adopted in thermochemical calculation is obviously key on determining the quench level of the species of interest. Wang et al. (2016) compared the chemical schemes of Moses et al. (2011) and Venot et al. (2012) in applications to Jupiter and Saturn. They found that these two schemes resulted in differences of about an order of magnitude on the abundance of CO, all other parameters and deep composition being kept similar. Moses (2014) already pointed out a significant difference in their carbon-oxygen chemistry, identifying a methanol (CH_3OH) conversion reaction as the main responsible. Venot et al. (2020) fully revised their CH_3OH chemistry, adopting recent experimental results of Burke et al. (2016). The new scheme was validated over a wide range of temperature and pressure.
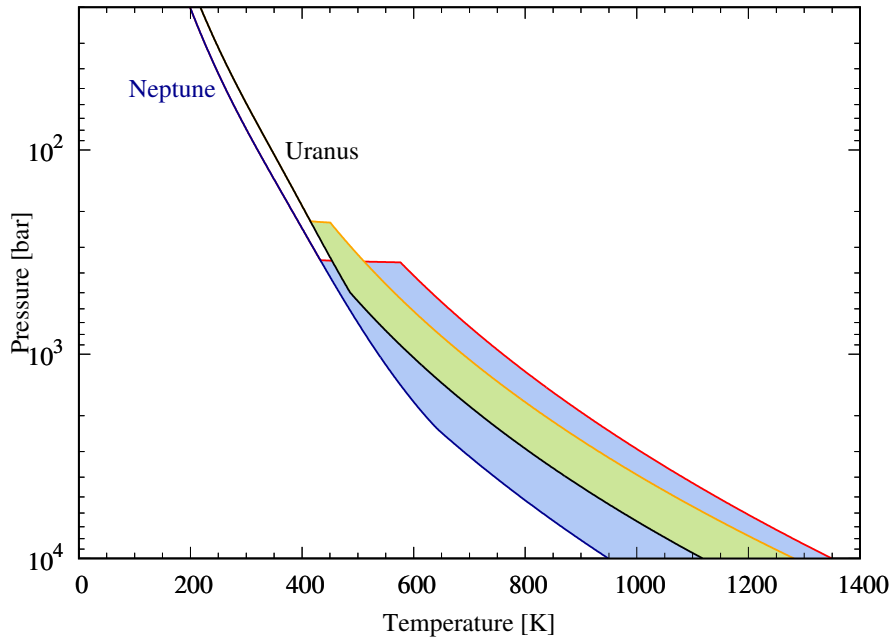
Fig. 2 Range of possible temperature profiles in the tropospheres of Uranus and Neptune, following Leconte et al. (2017) and Cavalié et al. (2017). The coldest profiles, corresponding to the wet adiabat, are shown in black (Uranus) and dark blue (Neptune). The warmest profiles, corresponding to the "3-layer profile", are shown in orange (Uranus) and red (Neptune). The filled areas (green for Uranus and blue for Neptune) indicate the range of possible temperatures.

The main changes concern the replacement of the reaction outlined by Moses (2014) by a more detailed mechanism, in which pressure dependent reaction rates are adopted. Planets in which CO quenching occurs at high pressures are affected by the modifications. For Uranus and Neptune, the effect of this update is to lower the CO quenching level towards higher pressures, compared to the results obtained with the chemical scheme of Venot et al. (2012). Consequently, to reproduce observational constraints of CH_4 and CO in the upper troposphere, a lower amount of H_2O is required in the deep tropospheric region where thermochemical equilibrium prevails. The O/H values found by Cavalié et al. (2017) using Venot et al. (2012)'s chemical scheme have been revised downwards. The O/H ratios necessary to reproduce current observations are <45 and 250 times protosolar value, for Uranus and Neptune respectively (Table 2).

Chemical schemes currently used to model tropospheres of the ice giants contains only species made of C, H, O, and N. However, the recent detection of H_2S in Uranus and Neptune (Irwin et al., 2018, 2019b) make really necessary the addition of sulphur species. Such models would then require to account for cloud formation (Atreya and Wong, 2005) as H_2S is involved in the formation of an NH_4SH cloud which consumes all NH_3 at these levels, and of an H_2S cloud above. Although not detected in ice giants, PH_3 might be present in these atmospheres also, as it is in Jupiter and Saturn. Alternately, its absence may serve as additional constraints for the deep oxygen abundance (Visscher and Fegley, 2005). The addition

of phosphorous species in chemical schemes is one of the next necessary step concerning the improvement of chemical schemes used to study ice giant atmospheres.

As we said in Sect. 3.5.1, the heterogeneity of the troposphere, as seen in disk-resolved tropospheric observations, makes necessary the development of GCMs including a detailed chemistry. Full chemical schemes are too heavy ($\sim$100 species and $\sim$2000 reactions) to be incorporated in 3D models, as it would result to unreasonable computational time. The solution is to include a reduced chemical scheme, valid for a limited number of species of interest. In this purpose, reduced schemes have already been proposed by Venot et al. (2019, 2020) for H, C, N and O species. Such reduced schemes must be regularly updated, e.g. to account for sulphur and phosphorus species.

3.5.4 Summary

Cavalié et al. (2017) have shown the range of O/H values one can derive for Uranus and Neptune given the current limited knowledge of several key parameters in thermochemical modeling. Future progress in deep composition derivation from thermochemical modeling of the troposphere of the ice giants require improvements to be made on the knowledge of the parameters this kind of models rely on. A better understanding of the 3D dynamics and chemistry to better constrain the disk variability of vertical mixing and temperature, both crucial in fixing quench levels, will involve a combination of disk-resolved observations, chemical and general circulation modeling work. Chemical networks will need to be extended to other key element bearing species and will have to include phase change processes for condensible species. Reaction rates for which either the temperature validity range or the accuracy are insufficient will need to be identified and improved (see e.g. Dobrijevic et al., 2010).

4 Thermochemical modeling in support of an ice giant atmospheric probe mass spectrometer

In this Section, we will briefly remind the baseline objectives of an ice giant mass spectrometer. We will then present the synergistic coupling of mass spectrometry with thermochemical modeling, and the requirements on the instrument such coupling drives. We will finally show how increasing the probe penetration depth could improve the science return of the probe mission. More details on the possible mass spectrometer can be found in Vorburger et al. (2020).

4.1 Baseline ice giant probe mass spectrometer

In the current baseline scenario proposed for ice giant atmospheric probes (e.g. Mousis et al. 2018 and Vorburger et al. 2020, and references therein), inherited from recent Saturn probe proposals (Mousis et al., 2014a, 2016; Atkinson et al., 2016, 2018), the nominally targeted depth is the 10-bar level. The mass spectrometer proposed for the Hera mission to Saturn and that is now considered for an ice giant probe mission consisted of several units, among which a time-of-flight mass spectrometer (TOF-MS) which has a nominal mass resolution of $\sim$1000 used for neutral gas composition, and a tunable laser spectrometer used for selected isotopic ratio measurements (Mousis et al., 2016; Wurz et al., 2012). The TOF-MS will

be 1000 times more sensitive than the Ion and Neutral Mass Spectrometer of the Cassini mission.

Reaching the 10-bar level with such an instrument will ensure accurate measurements of helium (within 2%) and the other noble gases (within 10%) that are expected to be well-mixed in both altitude and latitude. If the entry latitude is close to the equator, where methane is most abundant (see Section 2.1.2), the probe may also measure a carbon abundance representative of the deep C/H value. However Juno has shown with NH_3 that the well-mixed region for condensible species can occur much below than the cloud base of that species (Bolton et al., 2017; Li et al., 2017).

It will also measure the abundance of sulphur above the NH_4SH cloud, and thus the minimum S/N. However, N/H and S/H will remain out of reach, as the NH_4SH cloud deck is expected at 40 bars or so. Oxygen will also remain out of reach for a direct measurement, as water condenses as deep as a few hundred bars already in the ice giants (Atreya and Wong, 2005; Cavalié et al., 2017).

4.2 Synergistic coupling of in situ mass spectrometry and thermochemical modeling in ice giants

During its descent in the upper troposphere of an ice giant, the probe mass spectrometer will be sensitive to several gases (beyond helium, nobles gases, and methane) of key importance to constrain the deep composition of the ice giant from thermochemical modeling, provided that more ambitious mass resolution requirements are fulfilled.

The first species of interest is CO especially in Uranus, where its tropospheric component has not yet been unambiguously identified (Encrenaz et al., 2004; Cavalié et al., 2014). Combining mass spectrometry determination of the CO abundance within 10%, accurate temperature-pressure measurements of the Atmospheric Structure Instrument (Ferri and colleagues, 2019), and thermochemical modeling as detailed in Section 3, it will be possible to constrain the deep O/H of the ice giants more accurately than possible before. One limitation though regarding the deep O/H derivation is the single entry point of the probe which will result in a single temperature-pressure profile. Any variability over the planet, that is likely to occur, will remain out of reach to the probe. One key will then consist in picking the probe entry point such that we get a profile which is as much as possible representative for the whole planet by trajectory design and by knowing what places to avoid (e.g., avoid Great Dark Spots).

But directly measuring the abundance of CO bears several implications for the mass spectrometer. First, carbon dioxide (CO_2) needs also to be measured accurately as well as its fragmentation into CO inside the instrument. As CO_2 has the same mass as propane (C_3H_8), a mass resolution $m/\Delta m > 600$ is already required. Moreover, the instrument must be able to mass-separate CO from dinitrogen (N_2) and ethylene (C_2H_4). These species all reside at mass 28 on a mass spectrum. To separate them, a mass resolution $m/\Delta m > 3000$ is required at comparable abundance of CO and N_2.

As already stated in 2.1.5, additional constraints on the deep O/H can be obtained from measuring the abundance of PH_3 by solving the following thermochemical equation:

$$4PH_3 + 6H_2O = P_4O_6 + 12H_2. \tag{5}$$
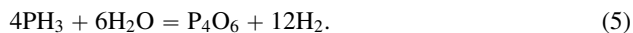
This would, in turn, require a mass resolution $m/\Delta m > 4000$, or a suitable chemical pre-separation (Vorburger et al., 2020), to separate PH_3 from H_2S, another mass-34 species detected in both ice giants. In the same spirit, ethane (C_2H_6) and acetylene (C_2H_2) can also
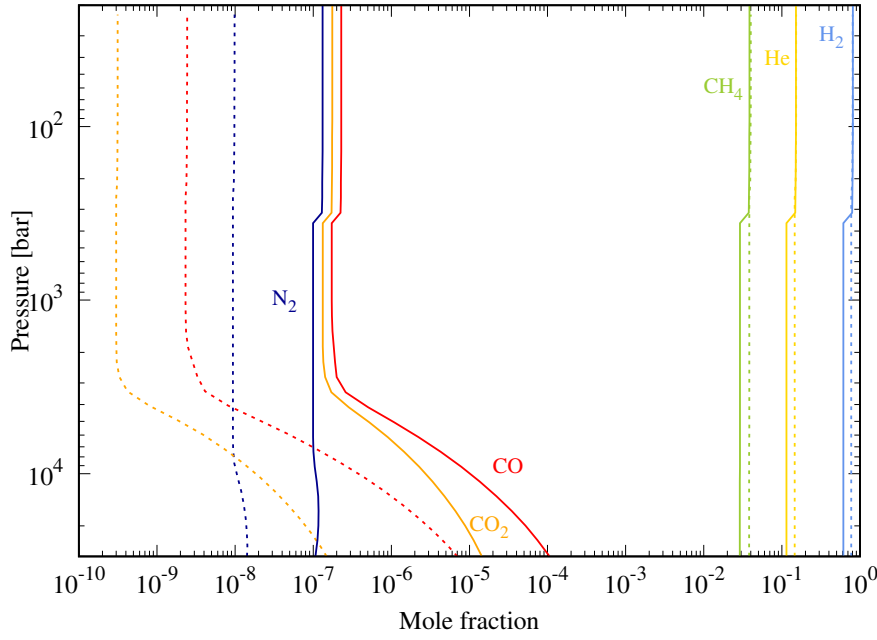
Fig. 3 Vertical profiles of CO (red), CO_2 (orange) and N_2 (dark blue) for Uranus (dashed lines) and Neptune (solid lines). Other main species like H_2, He and CH_4 are also shown with the corresponding layout.

be used as an additional constraint in the carbon-oxygen thermochemistry (Fegley and Prinn, 1985; Fegley and Lodders, 1994).

The direct benefit of such a high mass resolution would be a measurement of the N_2 abundance. In the same way CO is used to constrain the deep H_2O, N_2 can be used in thermochemical modeling to reproduce its upper tropospheric abundance and constrain the deep NH_3 abundance and thus the deep N/H, without the need for the probe to go beneath the NH_4SH cloud deck. Fig. 3 shows the vertical profiles of CO and N_2 for Uranus and Neptune using the model described in Venot et al. (2020) and assuming the deep N/H of Table 1. It shows that N_2 could be present in both planets with abundances comparable or even higher than CO. Having the deep N/H established this way, it would then be possible to derive the deep S/H from the combined reconstruction of the deep NH_3 and H_2S abundance profiles below the NH_4SH cloud deck and current H_2S observations above its own cloud (Irwin et al., 2018, 2019b). The current limitation of a descent probe in ice giants to measure directly N/H and S/H because of end-of-operations at 10 bars, i.e. before reaching the NH_4SH cloud deck at 40 bars or so, would thus be waived.

4.3 The question of depth

It is obvious that even more robust N/H and S/H values could be directly measured by an ice giant probe mass spectrometer, provided that it would reach below the NH_4SH cloud. However, such a depth goal bears implications on several technical aspects.

The descent would take longer to reach this level rather than the 10-bar level. The relay spacecraft would thus have to fly slower above the entry point to keep the radio link with the probe. For an orbiter, this would imply a higher orbit. However, placing the relay spacecraft further away from the probe would degrade the data rate. The situation on the data rate side is even more challenging as the atmospheric opacity increases exponentially with depth, especially beyond 15 bars, even though the situation is less critical now that it has been established that the main absorber in the altitude range will be H_2S rather than NH_3. To overcome this problem, two possibilities are being discussed: a second relay spacecraft could be sent or the communication system could use optical laser instead of radio frequencies.

4.4 The question of the probe entry latitude

To measure abundances of major species that are representative of their deep values, a probe should target an entry site where the material is uniformly mixed. There is already observational evidence that the high latitude may be depleted, at least in the upper troposphere, in CH_4 and H_2S (Sromovsky et al., 2014; Irwin et al., 2019a; Tollefson et al., 2019a). This, in turn, implies targeting latitudes where tropospheric mixing is maximum, i.e. the low latitudes in the ice giants according to Fig. 1. For disequilibrium species, which are quenched in layers where their abundance increase with depth (e.g., CO and PH_3), to be more likely detected by a mass spectrometer, low latitudes should also be favored. It should be noted however that there are some disequilibrium species (e.g., AsH_3) for which high latitudes should be more favorable.

Now that we have reviewed how the bulk composition of the ice giants can be constrained from the combination of in situ measurements and thermochemical modeling (possibly supplemented by remote sensing observations), we will review how it can help us better understand the interior of these planets and the processes that led to their formation.

5 Link between deep composition, interior models, and planet formation

Because the atmospheres and interiors of the giant planets are intimately linked and there is no probe that can go very deep into either planet, a proper understanding of Uranus and Neptune's atmospheres is crucial to characterise their interiors. The atmospheric thermal profiles and deep compositions put constraints and impact directly on the interior model calculations (Guillot, 2005; Guillot and Gautier, 2015; Helled and Guillot, 2018).

The internal structure of Uranus and Neptune is estimated using interior models that fit the observational data for mass, radius, luminosity, atmospheric temperature, atmospheric abundances and gravity data. With only one mission (Voyager 2) visiting these planets so far, the gravity data that was obtained by remote sensing is much more limited than what we have for Jupiter (Bolton et al., 2017; Iess et al., 2018) and Saturn (Iess et al., 2019). In Table 5, we show the parameters used for interior model calculations for Uranus and Neptune with the exception of the atmospheric abundances, already shown in Table 1. The data for Jupiter and Saturn are shown for comparison.

The information in Table 5 is combined with interior models to calculate the mass of heavy elements and their distribution in the interior, investigating all possible interior structures for Uranus and Neptune (see Section 5.2). Given that one of the most accepted theories for the formation of these planets requires that a core forms first and the gas is accreted later

Parameter	Jupiter	Saturn	Uranus	Neptune
Mass/10^{24} (kg)	1898.187 ± 0.088[a]	568.336 ± 0.026[b]	86.8127 ± 0.0040[c]	102.4126 ± 0.0048[d]
Equatorial radius (km)	71492 ± 4[e]	60268 ± 4[e]	25559 ± 4[e]	24764 ± 15[e]
Temperature$_{1bar}$ (K)	165 ± 4[f]	135 ± 5[f]	76 ± 2[f]	72 ± 2[f]
Intrinsic flux ($J\ s^{-1}\ m^{-2}$)	5.44 ± 0.43[g]	2.01 ± 0.14[g]	$0.042^{+0.047}_{-0.042}$[g]	0.433 ± 0.046[g]
$J_2/10^6$	14696.572 ± 0.0046[h]	16290.573 ± 0.0093[i]	3516 ± 3.2[j]	3408.4 ± 3404.5[d]
$J_3/10^6$	-0.042 ± 0.0033[h]	0.059 ± 0.0076[i]	−	−
$J_4/10^6$	-586.609 ± 0.0013[h]	-935.314 ± 0.0123[i]	-35.4 ± 34.1[j]	-33.4 ± 32.9[d]
$J_5/10^6$	-0.069 ± 0.0026[h]	-0.224 ± 0.018[i]	−	−
$J_6/10^6$	34.198 ± 0.003[h]	86.340 ± 0.029[i]	−	−
$J_7/10^6$	0.124 ± 0.0056[h]	−	−	−
$J_8/10^6$	-2.426 ± 0.0083[h]	-14.624 ± 0.0683[i]	−	−
$J_9/10^6$	-0.106 ± 0.0146[h]	−	−	−
$J_{10}/10^6$	0.172 ± 0.023[h]	4.672 ± 0.14[i]	−	−
$J_{12}/10^6$	−	-0.997 ± 0.224[i]	−	−

[a] Jacobson 2003 - published in the JPL website: https://ssd.jpl.nasa.gov/?planet_phys_par
[b] Jacobson et al. (2006)
[c] Jacobson (2014)
[d] Jacobson (2009)
[e] Archinal et al. (2018)
[f] Lindal (1992), note that Seiff et al. (1998) derived 166.1 K for Jupiter
[g] Pearl and Conrath (1991)
[h] Iess et al. (2018)
[i] Iess et al. (2019)
[j] Lindal et al. (1981), Helled and Guillot (2013) derive slightly different values

on (see Section 5.1), the constraints obtained from the interior models are crucial to understand the history of these planets.

Uranus and Neptune are usually referred to as twin planets, but in reality they have many differences. When looking at their masses and radii we notice that Neptune is denser than Uranus, by approximately 30%. The reason for this difference is not clear, but it was suggested that giant impacts during their formation and evolution might have affected their structure (Podolak and Helled, 2012). Uranus has a much higher obliquity when compared with Neptune and all the other giants, that is also explained with a giant impact during its formation, and that may cause differences in the atmospheres between the two ice giants (Safronov, 1966). In addition, Table 5 shows that the intrinsic flux of these two planets is quite different. While Neptune emits more energy than it receives from the Sun, Uranus has an emitted flux an order of magnitude lower than its neighbour. This implies that while Neptune is still cooling, Uranus is almost in equilibrium with the solar irradiation, which implies differences in the energy transport in their interiors and points towards different evolution for these two planets.

Regarding the link between the atmosphere and interior, one of the most important constraints needed for interior models are the atmospheric abundances, which have been extensively discussed in the previous Sections. Uranus and Neptune are different from Jupiter and Saturn because they are not merely dominated by hydrogen and helium, and may be highly enriched in heavy elements. While H and He are consistent with the protosolar abundances, C has an enrichment of 80 ± 20 compared to the protosun (Atreya et al., 2018), but this may as well be a lower limit only.

Another relevant parameter used in interior models is the temperature at 1 bar, that sets the upper boundary for these calculations. This parameter is obtained from stellar and ring occultations, that also provides determination of the shape of the planets. However, we have

to note that this data are limited to low-pressure values, approximately 0.1 bar and even lower pressures (French et al., 1998), and this can bring uncertainties in the radius used to model these planets (Helled et al., 2010). In addition to this, the thermal profile inferred to reach the 1 bar level is highly degenerate (it depends on many unknown parameters such as the refractivity which depends on the mean molecular weight and the temperature at each pressure level). Therefore, the temperature inferred corresponds to one possible solution, but there might be other possibilities (Guillot, 1995; Sromovsky et al., 2011).

The magnetic field is another observable quantity that provides constraints to understand the boundary between the deep atmosphere and the interior. Observations suggest that there is a convective and electrically conductive region that extends down to 20% of the radius (Stanley and Bloxham, 2004, 2006; Redmer et al., 2011). This is directly linked with the dynamics of Uranus and Neptune's atmospheres, with zonal winds that extend down to approximately 1000 km below the clouds (Kaspi et al., 2013) and putting constraints on the interior models and linking it with the deep atmosphere.

5.1 Formation theories

The most accepted scenario to explain the formation of the giant planets is the core accretion model, where the planets grow first their cores and then, once they reach a critical core mass, start accreting gas and forming their gaseous envelopes (Pollack et al., 1996). There are different theories to explain how the core was first formed, that can be either by accreting planetesimals, bodies of some km in size (e.g. Alibert et al., 2005), or by pebbles of some mm to cm in size (e.g. Lambrechts and Johansen, 2014). Regarding their gaseous envelope, once the critical core mass is reached, the giant planets start accreting gas in a runaway fashion, and one of the long standing questions in the case of Uranus and Neptune is how to stop such gas accretion to prevent them of accreting a massive gaseous envelope and becoming gas giants. One of the ideas to solve this problem suggests that, in a planetesimal-driven scenario, the planets formed in a region with a smaller density of solids when compared to where Jupiter and Saturn were formed. Their cores therefore grew slowly enough for the protoplanetary disk to be almost dissipated by the time the protoplanets started the gas accretion phase. This is why they are sometimes referred as "failed giants" (Pollack et al., 1996; Helled et al., 2014). Other ideas require fine tuning of the models to prevent the planets of entering the gas accretion mode (Frelikh and Murray-Clay, 2017).

The other theory to explain the formation of these planets is the disk instability. According to this scenario, clumps formed in the protosolar disk due to gravitational instabilities that gave rise to the giant planets. Uranus and Neptune could have been formed in this scenario if there was substantial gaseous mass loss in the disk caused by tidal stripping or photo-evaporation (see Helled and Bodenheimer 2014 and references therein).

Given the different possible scenarios and competing theories, interior model calculations are crucial to disentangle these competing scenarios, and thus better understand the formation and evolution of these planets.

5.2 Internal Structure of Uranus and Neptune

Interior models are constructed assuming hydrostatic, thermodynamic, mass and energy conservation, solving the following set of differential equations:

$$\frac{\partial P}{\partial r} = -\rho \, g \tag{6}$$

Uranus **Neptune**

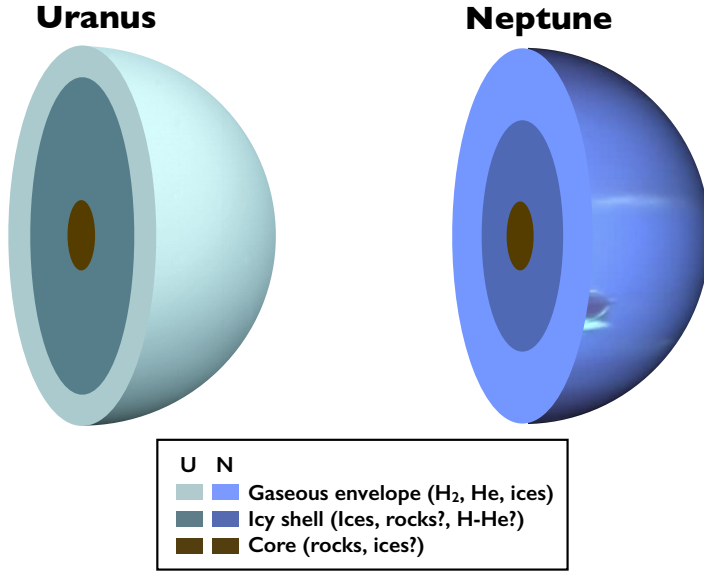| U	N	
		Gaseous envelope (H₂, He, ices)
		Icy shell (Ices, rocks?, H-He?)
		Core (rocks, ices?)

Fig. 4 Schematic view of Uranus and Neptune's interior structures.

$$\frac{\partial T}{\partial r} = \frac{\partial P}{\partial r}\frac{T}{P}\nabla_T \tag{7}$$

$$\frac{\partial m}{\partial r} = 4\pi r^2 \rho \tag{8}$$

$$\frac{\partial L}{\partial r} = 4\pi r^2 \rho \left(\dot{\epsilon} - T\frac{\partial S}{\partial t}\right) \tag{9}$$

with P the pressure, r the radius, ρ the density, g the gravitational acceleration, T the temperature, m the mass, L the planet luminosity and S its entropy.

Given the poor gravity constraints for these planets (see Table 5), one of the major obstacles found when modeling their interiors and constraining the ice-to-rock ratio is the significant degeneracies in their potential composition (Podolak et al., 1991; Hubbard et al., 1995; Baraffe et al., 2014). Some of the structure models for Uranus and Neptune use three fully adiabatic layers (a rocky core, an icy shell and a gaseous envelope) and *ab initio* equations of state (EOS) (Nettelmann et al., 2013). Nevertheless, other methods using no pre-stablished assumption regarding the structure or equations of state (e.g. Marley et al., 1995; Helled et al., 2011) also proved to be useful. All these approaches find that the heavy element concentration increases towards the planetary centre, as shown by Fig. 4. Note that Fig. 4 is a schematic representation where there are sharp boundaries between the different layers, but a more realistic idea is to consider a gradient of heavy elements and change in composition towards the interior (Helled and Guillot, 2018) (see also Section 5.3). More specific values for the metallicities in the gaseous envelope and the icy shell can be found in Fig. 5, which
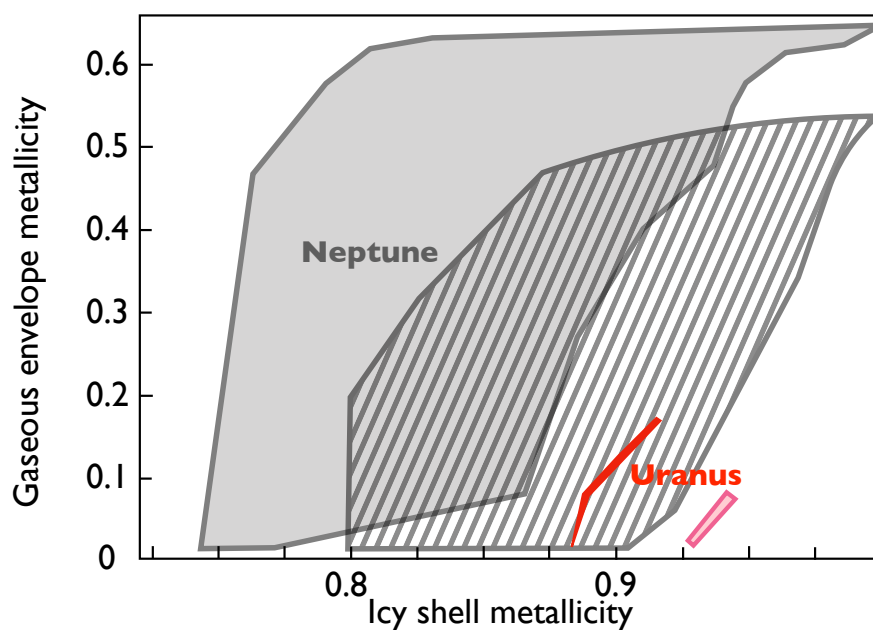
Fig. 5 Heavy elements mass fraction in the icy shell vs. the gaseous envelope. Structure models solutions for Uranus models are shown in red and for Neptune in grey (dashed). Models with a modified shape and rotation data for Uranus (pink) and Neptune (solid grey) are also shown. Adapted from Nettelmann et al. (2013).

shows results found by Nettelmann et al. (2013). As seen in Fig. 5, there are still big uncertainties in the internal structure of these planets. Some of the uncertainties are related to the fact that the core mass, the ice-to-rock ratio, the equations of state of mixtures of materials, the pressure of separation between the different layers, the depth of the winds and extent of differential rotation and the extent of compositional gradients, are highly unknown for these planets. Because the observational data are crucial to tackle these degeneracies, a more accurate determination of the gravity field and a proper characterization of the atmospheres of Uranus and Neptune are needed to get a better knowledge of their interior structures.

5.3 Remaining questions and challenges for the future

Despite the substantial progress in the modeling of planetary interiors in the last decades, there are still several unsolved questions regarding the nature of Uranus and Neptune. One of the most important parameters when modeling the interior of these planets is EOS. In the last decade, there has been great progress in this area, with new EOS published for hydrogen and helium (Militzer and Hubbard, 2013; Becker et al., 2014; Chabrier et al., 2019) and also in heavier material such as water (Nettelmann et al., 2008; Mazevet et al., 2019). Nevertheless, disagreement between the different EOS still cause differences in the internal structure of these planets (e.g. Miguel et al. 2016 for Jupiter), and better constraints on EOS not only of individual elements but also in mixtures, together with higher pressure experiments could deeply improve interior structure models. Another important aspect of the interior modeling

is the energy transport mechanism. The source of the different cooling rates of the planets is still unsolved. Better modeling, especially with potentially non-adiabatic models and a more realistic distribution of heavy elements in the interior, could help unveiling this story (Helled and Guillot, 2018; Vazan and Helled, 2020). Last but not least, we need to understand the bulk composition of these planets: are they really formed by ices or do they have a substantial amount of rocks in their interiors? And how are these heavy elements distributed? These are questions that are far from being solved.

When thinking of formation mechanisms, there are still several key questions that remain open: Where in the primitive nebula were Uranus and Neptune formed? Was pebble accretion or planetesimal accretion the primary mechanism that formed their cores? What are the mechanisms at play regarding gas accretion? What is the enrichment of the gaseous envelope and the radial distribution of heavy elements during the planet formation and subsequent evolution? Understanding the connection between the atmosphere, interior and link with formation of these planets is still incomplete and one of the big challenges in planetary science for the future. New studies on the deposition of heavy elements in the forming giant planet (Valletta and Helled, 2019) and recent results in exoplanet studies indicate that measurements of the envelope metallicities are relevant diagnostics of the bulk metallicity (Thorngren and Fortney, 2019). Measurements from the Earth, but more importantly, at least for the gravity data and bulk composition, future space missions to Uranus and Neptune carrying in situ probes will provide constraints to reduce the degeneracies in calculations towards a better understanding on the atmosphere-interior connection, on the internal structure and ultimately the history of these worlds.

6 Conclusion

An entry probe is the only means to measure the deep abundance of a number of species of key importance, notably the noble gases. These can put significant constraints on formation of Uranus and Neptune (Mousis et al., 2018). The difficulty with those cold distant worlds lies in the condensation of some key species, like CH_4, and to a more critical extent, H_2S, NH_3, and H_2O, which render their direct in situ measurement complicated, or even impossible.

Designing a probe that would reach the 40-50 bar level and return data to measure not only He/H (and other noble gases) and C/H, but also N/H and S/H, will be very challenging in the current timeframe (possible launch dates range from 2029 to 2034, Simon et al. 2020). The coupling of high resolution mass spectrometry ($m/\Delta m > 4000$) with accurate temperature-pressure measurements with thermochemical modeling at 10 bar is thus an interesting combination to infer the deep elemental abundances of condensible species not reachable by a shallow probe, like H_2O, NH_3 and H_2S, in the ice giants.

The results of such an entry probe, combined with a better knowledge of gravity moments and magnetic field obtained from an orbiter, will undoubtedly result in major breakthroughs in our understanding of the formation and evolution of the ice giants of our Solar System, Uranus and Neptune.

References

Ali-Dib M, Mousis O, Petit JM, Lunine JI (2014) The Measured Compositions of Uranus and Neptune from their Formation on the CO Ice Line. Astrophys. J. 793:9, DOI 10.1088/0004-637X/793/1/9

Alibert Y, Mordasini C, Benz W, Winisdoerffer C (2005) Models of giant planet formation with migration and disc evolution. Astron. Astrophys. 434(1):343–353, DOI 10.1051/0004-6361:20042032

Amarsi AM, Asplund M (2017) The solar silicon abundance based on 3D non-LTE calculations. Mon. Not. R. Astron. Soc. 464(1):264–273, DOI 10.1093/mnras/stw2445

Amarsi AM, Barklem PS, Asplund M, Collet R, Zatsarinny O (2018) Inelastic O+H collisions and the O I 777 nm solar centre-to-limb variation. Astron. Astrophys. 616:A89, DOI 10.1051/0004-6361/201832770

Amarsi AM, Barklem PS, Collet R, Grevesse N, Asplund M (2019) 3D non-LTE line formation of neutral carbon in the Sun. Astron. Astrophys. 624:A111, DOI 10.1051/0004-6361/201833603

Archinal BA, Acton CH, AHearn MF, Conrad A, Consolmagno GJ, Duxbury T, Hestroffer D, Hilton JL, Kirk RL, Klioner SA, McCarthy D, Meech K, Oberst J, Ping J, Seidelmann PK, Tholen DJ, Thomas PC, Williams IP (2018) Report of the IAU Working Group on Cartographic Coordinates and Rotational Elements: 2015. Celest Mech Dyn Astr 130:22, DOI 10.1007/s10569-017-9805-5

Arridge CS, Achilleos N, Agarwal J, Agnor CB, Ambrosi R, André N, Badman SV, Baines K, Banfield D, Barthélémy M, Bisi MM, Blum J, Bocanegra-Bahamon T, Bonfond B, Bracken C, Brandt P, Briand C, Briois C, Brooks S, Castillo-Rogez J, Cavalié T, Christophe B, Coates AJ, Collinson G, Cooper JF, Costa-Sitja M, Courtin R, Daglis IA, de Pater I, Desai M, Dirkx D, Dougherty MK, Ebert RW, Filacchione G, Fletcher LN, Fortney J, Gerth I, Grassi D, Grodent D, Grün E, Gustin J, Hedman M, Helled R, Henri P, Hess S, Hillier JK, Hofstadter MH, Holme R, Horanyi M, Hospodarsky G, Hsu S, Irwin P, Jackman CM, Karatekin O, Kempf S, Khalisi E, Konstantinidis K, Krüger H, Kurth WS, Labrianidis C, Lainey V, Lamy LL, Laneuville M, Lucchesi D, Luntzer A, MacArthur J, Maier A, Masters A, McKenna-Lawlor S, Melin H, Milillo A, Moragas-Klostermeyer G, Morschhauser A, Moses JI, Mousis O, Nettelmann N, Neubauer FM, Nordheim T, Noyelles B, Orton GS, Owens M, Peron R, Plainaki C, Postberg F, Rambaux N, Retherford K, Reynaud S, Roussos E, Russell CT, Rymer AM, Sallantin R, Sánchez-Lavega A, Santolik O, Saur J, Sayanagi KM, Schenk P, Schubert J, Sergis N, Sittler EC, Smith A, Spahn F, Srama R, Stallard T, Sterken V, Sternovsky Z, Tiscareno M, Tobie G, Tosi F, Trieloff M, Turrini D, Turtle EP, Vinatier S, Wilson R, Zarka P (2014) The science case for an orbital mission to Uranus: Exploring the origins and evolution of ice giant planets. Planet. Space Sci. 104:122–140, DOI 10.1016/j.pss.2014.08.009

Atkinson DH, Simon AA, Banfield D, Atreya SK, Blacksberg J, Brinckerhoff W, Colaprete A, Coustenis A, Fletcher L, Guillot T, Hofstadter M, Lunine JI, Mahaffy P, Marley MS, Mousis O, Spilker TR, Trainer MG, Webster C (2016) Exploring Saturn - The Saturn PRobe Interior and aTmosphere Explorer (SPRITE) Mission. In: AAS/Division for Planetary Sciences Meeting Abstracts, AAS/Division for Planetary Sciences Meeting Abstracts, vol 48, p #123.29

Atkinson DH, Simon A, Banfield D, Atreya S, Blacksberg J, Brinckerhoff W, Colaprete A, Coustenis A, Fletcher L, Guillot T, Hofstadter M, Lunine J, Mahaffy P, Marley M, Mousis O, Spilker T, Trainer M, Webster C (2018) SPRITE (Saturn PRobe Interior and aTmosphere Explorer): A Saturn Entry Probe Mission Concept. In: European Planetary

Science Congress, pp EPSC2018–65

Atreya SK, Wong AS (2005) Coupled Clouds and Chemistry of the Giant Planets— A Case for Multiprobes. Space Sci. Rev. 116(1-2):121–136, DOI 10.1007/s11214-005-1951-5

Atreya SK, Wong MH, Owen TC, Mahaffy PR, Niemann HB, de Pater I, Drossart P, Encrenaz T (1999) A comparison of the atmospheres of Jupiter and Saturn: deep atmospheric composition, cloud structure, vertical mixing, and origin. Planet. Space Sci. 47:1243–1262, DOI 10.1016/S0032-0633(99)00047-1

Atreya SK, Mahaffy PR, Niemann HB, Wong MH, Owen TC (2003) Composition and origin of the atmosphere of Jupiter - an update, and implications for the extrasolar giant planets. Planetary and Space Science 51(2):105–112, DOI 10.1016/S0032-0633(02)00144-7

Atreya SK, Crida A, Guillot T, Lunine JI, Madhusudhan N, Mousis O (2018) The Origin and Evolution of Saturn, with Exoplanet Perspective, Cambridge University Press, p 5?43. Cambridge Planetary Science, DOI 10.1017/9781316227220.002

Atreya SK, Hofstadter MH, In JH, Mousis O, Reh K, Wong MH (2020) Deep Atmosphere Composition, Structure, Origin, and Exploration, with Particular Focus on Critical in situ Science at the Icy Giants. Space Sci. Rev. 216(1):18, DOI 10.1007/s11214-020-0640-8

Baines KH, Mickelson ME, Larson LE, Ferguson DW (1995) The abundances of methane and ortho/para hydrogen on Uranus and Neptune: Implications of New Laboratory 4-0 H2 quadrupole line parameters. Icarus 114:328–340, DOI 10.1006/icar.1995.1065

Bar-Nun A, Kleinfeld I, Kochavi E (1988) Trapping of gas mixtures by amorphous water ice. Phys. Rev. B 38:7749–7754, DOI 10.1103/PhysRevB.38.7749

Baraffe I, Chabrier G, Fortney J, Sotin C (2014) Planetary Internal Structures. In: Beuther H, Klessen RS, Dullemond CP, Henning T (eds) Protostars and Planets VI, p 763, DOI 10.2458/azu_uapress_9780816531240-ch033

Becker A, Lorenzen W, Fortney JJ, Nettelmann N, Schöttler M, Redmer R (2014) Ab Initio Equations of State for Hydrogen (H-REOS.3) and Helium (He-REOS.3) and their Implications for the Interior of Brown Dwarfs. Astrophys. J. Suppl. 215(2):21, DOI 10.1088/0067-0049/215/2/21

Beer R (1975) Detection of carbon monoxide in Jupiter. Astrophys. J. Lett. 200:L167–L169, DOI 10.1086/181923

Bézard B, Griffith CA, Kelly DM, Lacy JH, Greathouse T, Orton G (1997) Thermal Infrared Imaging Spectroscopy of Shoemaker-Levy 9 Impact Sites: Temperature and HCN Retrievals. Icarus 125(1):94–120, DOI 10.1006/icar.1996.5610

Bézard B, Feuchtgruber H, Moses JI, Encrenaz T (1998) Detection of methyl radicals (CH_3) on Saturn. Astron. Astrophys. 334:L41–L44

Bézard B, Romani PN, Feuchtgruber H, Encrenaz T (1999) Detection of the Methyl Radical on Neptune. Astrophys. J. 515(2):868–872, DOI 10.1086/307070

Bézard B, Lellouch E, Strobel D, Maillard JP, Drossart P (2002) Carbon Monoxide on Jupiter: Evidence for Both Internal and External Sources. Icarus 159:95–111, DOI 10.1006/icar.2002.6917

Bolton SJ, Adriani A, Adumitroaie V, Allison M, Anderson J, Atreya S, Bloxham J, Brown S, Connerney JEP, DeJong E, Folkner W, Gautier D, Grassi D, Gulkis S, Guillot T, Hansen C, Hubbard WB, Iess L, Ingersoll A, Janssen M, Jorgensen J, Kaspi Y, Levin SM, Li C, Lunine J, Miguel Y, Mura A, Orton G, Owen T, Ravine M, Smith E, Steffes P, Stone E, Stevenson D, Thorne R, Waite J, Durante D, Ebert RW, Greathouse TK, Hue V, Parisi M, Szalay JR, Wilson R (2017) Jupiter's interior and deep atmosphere: The initial pole-to-pole passes with the Juno spacecraft. Science 356(6340):821–825, DOI 10.1126/science.aal2108

Boss AP (1997) Giant planet formation by gravitational instability. Science 276:1836–1839, DOI 10.1126/science.276.5320.1836

Boss AP (2002) Formation of gas and ice giant planets. Earth and Planetary Science Letters 202(3-4):513–523, DOI 10.1016/S0012-821X(02)00808-7

Bregman JD, Lester DF, Rank DM (1975) Observations of the ν_2 band of PH_3 in the atmosphere of Saturn. Astrophys. J. Lett. 202:L55, DOI 10.1086/181979

Briggs FH, Sackett PD (1989) Radio observations of Saturn as a probe of its atmosphere and cloud structure. Icarus 80(1):77–103, DOI 10.1016/0019-1035(89)90162-0

Burgdorf M, Orton GS, Davis GR, Sidher SD, Feuchtgruber H, Griffin MJ, Swinyard BM (2003) Neptune's far-infrared spectrum from the ISO long-wavelength and short-wavelength spectrometers. Icarus 164:244–253, DOI 10.1016/S0019-1035(03)00138-6

Burgdorf M, Orton G, van Cleve J, Meadows V, Houck J (2006) Detection of new hydrocarbons in Uranus' atmosphere by infrared spectroscopy. Icarus 184:634–637, DOI 10.1016/j.icarus.2006.06.006

Burke U, Metcalfe WK, Burke SM, Heufer KA, Dagaut P, Curran HJ (2016) A detailed chemical kinetic modeling, ignition delay time and jet-stirred reactor study of methanol oxidation. Combust. Flame 165:125–136

Cavalié T, Billebaud F, Biver N, Dobrijevic M, Lellouch E, Brillet J, Lecacheux A, Hjalmarson Å, Sandqvist A, Frisk U, Olberg M, Bergin EA, The Odin Team (2008) Observation of water vapor in the stratosphere of Jupiter with the Odin space telescope. Planet. Space Sci. 56:1573–1584, DOI 10.1016/j.pss.2008.04.013

Cavalié T, Billebaud F, Dobrijevic M, Fouchet T, Lellouch E, Encrenaz T, Brillet J, Moriarty-Schieven GH, Wouterloot JGA, Hartogh P (2009) First observation of CO at 345 GHz in the atmosphere of Saturn with the JCMT: New constraints on its origin. Icarus 203:531–540, DOI 10.1016/j.icarus.2009.05.024

Cavalié T, Hartogh P, Billebaud F, Dobrijevic M, Fouchet T, Lellouch E, Encrenaz T, Brillet J, Moriarty-Schieven GH (2010) A cometary origin for CO in the stratosphere of Saturn? Astron. Astrophys. 510:A88

Cavalié T, Biver N, Hartogh P, Dobrijevic M, Billebaud F, Lellouch E, Sandqvist A, Brillet J, Lecacheux A, Hjalmarson Å, Frisk U, Olberg M, Odin Team (2012) Odin space telescope monitoring of water vapor in the stratosphere of Jupiter. Planet. Space Sci. 61:3–14, DOI 10.1016/j.pss.2011.04.001

Cavalié T, Feuchtgruber H, Lellouch E, de Val-Borro M, Jarchow C, Moreno R, Hartogh P, Orton G, Greathouse TK, Billebaud F, Dobrijevic M, Lara LM, González A, Sagawa H (2013) Spatial distribution of water in the stratosphere of Jupiter from Herschel HIFI and PACS observations. Astron. Astrophys. 553:A21, DOI 10.1051/0004-6361/201220797

Cavalié T, Moreno R, Lellouch E, Hartogh P, Venot O, Orton GS, Jarchow C, Encrenaz T, Selsis F, Hersant F, Fletcher LN (2014) The first submillimeter observation of CO in the stratosphere of Uranus. Astron. Astrophys. 562:A33, DOI 10.1051/0004-6361/201322297

Cavalié T, Venot O, Selsis F, Hersant F, Hartogh P, Leconte J (2017) Thermochemistry and vertical mixing in the tropospheres of Uranus and Neptune. How convection inhibition can affect the derivation of deep oxygen abundances. Icarus 291:1–16

Cavalié T, Hue V, Hartogh P, Moreno R, Lellouch E, Feuchtgruber H, Jarchow C, Cassidy T, Fletcher LN, Billebaud F, Dobrijevic M, Rezac L, Orton GS, Rengel M, Fouchet T, Guerlet S (2019) Herschel map of Saturn's stratospheric water, delivered by the plumes of Enceladus. Astron. Astrophys. 630:A87, DOI 10.1051/0004-6361/201935954

Chabrier G, Mazevet S, Soubiran F (2019) A New Equation of State for Dense Hydrogen-Helium Mixtures. Astrophys. J. 872(1):51, DOI 10.3847/1538-4357/aaf99f

Connerney JEP (1986) Magnetic connection for Saturn's rings and atmosphere. Geophys. Res. Lett. 13:773–776, DOI 10.1029/GL013i008p00773

Connerney JEP, Waite JH (1984) New model of Saturn's ionosphere with an influx of water from the rings. Nature 312(5990):136–138, DOI 10.1038/312136a0

Conrath B, Hanel R, Gautier D, Marten A, Lindal G (1987) The helium abundance of Uranus from Voyager measurements. J. Geophys. Res. 92:15003–15010, DOI 10.1029/JA092iA13p15003

Conrath BJ, Gautier D (2000) Saturn Helium Abundance: A Reanalysis of Voyager Measurements. Icarus 144:124–134, DOI 10.1006/icar.1999.6265

Conrath BJ, Gautier D, Hanel RA, Hornstein JS (1984) The helium abundance of Saturn from Voyager measurements. The Astrophysical Journal 282:807–815, DOI 10.1086/162267

Conrath BJ, Gautier D, Lindal GF, Samuelson RE, Shaffer WA (1991) The helium abundance of Neptune from Voyager measurements. J. Geophys. Res. 96:18907

Conrath BJ, Gautier D, Owen TC, Samuelson RE (1993) Constraints on N_2 in Neptune's Atmosphere from Voyager Measurements. Icarus 101(1):168–171, DOI 10.1006/icar.1993.1014

Courtin R, Gautier D, Marten A, Bezard B, Hanel R (1984) The composition of Saturn's atmosphere at northern temperate latitudes from Voyager IRIS spectra - NH3, PH3, C2H2, C2H6, CH3D, CH4, and the Saturnian D/H isotopic ratio. Astrophys. J. 287:899–916, DOI 10.1086/162748

Courtin R, Pandey-Pommier M, Gautier D, Zarka P, Hofstadter M, Hersant F, Girard J (2015) Metric Observations of Saturn with the Giant Metrewave Radio Telescope. In: SF2A-2015: Proceedings of the Annual meeting of the French Society of Astronomy and Astrophysics, pp 241–245

de Pater I, Richmond M (1989) Neptune's microwave spectrum from 1 MM to 20 CM. Icarus 80:1–13, DOI 10.1016/0019-1035(89)90158-9

de Pater I, Romani PN, Atreya SK (1989) Uranus deep atmosphere revealed. Icarus 82(2):288–313, DOI 10.1016/0019-1035(89)90040-7

de Pater I, Romani PN, Atreya SK (1991) Possible microwave absorption by H2S gas in Uranus' and Neptune's atmospheres. Icarus 91:220–233, DOI 10.1016/0019-1035(91)90020-T

de Pater I, Sault RJ, Butler B, DeBoer D, Wong MH (2016) Peering through Jupiter's clouds with radio spectral imaging. Science 352(6290):1198–1201, DOI 10.1126/science.aaf2210

de Pater I, Butler B, Sault RJ, Moullet A, Moeckel C, Tollefson J, de Kleer K, Gurwell M, Milam S (2018) Potential for Solar System Science with the ngVLA. In: Murphy E (ed) Science with a Next Generation Very Large Array, Astronomical Society of the Pacific Conference Series, vol 517, p 49

de Pater I, Sault RJ, Wong MH, Fletcher LN, DeBoer D, Butler B (2019) Jupiter's ammonia distribution derived from VLA maps at 3-37 GHz. Icarus 322:168–191, DOI 10.1016/j.icarus.2018.11.024

DeBoer DR, Steffes PG (1994) Laboratory measurements of the microwave properties of H2S under simulated Jovian conditions with an application to Neptune. Icarus 109:352–366, DOI 10.1006/icar.1994.1099

DeBoer DR, Steffes PG (1996) Estimates of the Tropospheric Vertical Structure of Neptune Based on Microwave Radiative Transfer Studies. Icarus 123:324–335, DOI 10.1006/icar.1996.0161

Dobrijevic M, Cavalié T, Hébrard E, Billebaud F, Hersant F, Selsis F (2010) Key reactions in the photochemistry of hydrocarbons in Neptune's stratosphere. Planet. Space Sci. 58:1555–1566, DOI 10.1016/j.pss.2010.07.024

Dobrijevic M, Cavalié T, Billebaud F (2011) A methodology to construct a reduced chemical scheme for 2D-3D photochemical models: Application to Saturn. Icarus 214:275–285, DOI 10.1016/j.icarus.2011.04.027

Dobrijevic M, Loison JC, Hickson KM, Gronoff G (2016) 1D-coupled photochemical model of neutrals, cations and anions in the atmosphere of Titan. Icarus 268:313–339, DOI 10.1016/j.icarus.2015.12.045

Dobrijevic M, Loison JC, Hue V, Cavalié T, Hickson KM (2020) 1D photochemical model of the ionosphere and the stratosphere of Neptune. Icarus 335:113375, DOI 10.1016/j.icarus.2019.07.009

Drummond B, Tremblin P, Baraffe I, Amundsen DS, Mayne NJ, Venot O, Goyal J (2016) The effects of consistent chemical kinetics calculations on the pressure-temperature profiles and emission spectra of hot Jupiters. Astron. Astrophys. 594:A69, DOI 10.1051/0004-6361/201628799

Encrenaz T, Lellouch E, Drossart P, Feuchtgruber H, Orton GS, Atreya SK (2004) First detection of CO in Uranus. Astron. Astrophys. 413:L5–L9, DOI 10.1051/0004-6361:20034637

Fegley B, Prinn RG (1988) Chemical constraints on the water and total oxygen abundances in the deep atmosphere of Jupiter. The Astrophysical Journal 324:621–625, DOI 10.1086/165922

Fegley J B, Prinn RG (1985) Equilibrium and nonequilibrium chemistry of Saturn's atmosphere - Implications for the observability of PH3, N2, CO, and GeH4. Astrophys. J. 299:1067–1078, DOI 10.1086/163775

Fegley J B, Prinn RG (1986) Chemical Models of the Deep Atmosphere of Uranus. Astrophys. J. 307:852, DOI 10.1086/164472

Fegley J Bruce, Lodders K (1994) Chemical Models of the Deep Atmospheres of Jupiter and Saturn. Icarus 110(1):117–154, DOI 10.1006/icar.1994.1111

Ferri F, colleagues (2019) The atmospheric structure of the ice giants planets from in situ measurements. Space Sci. Rev. this issue

Feuchtgruber H, Lellouch E, de Graauw T, Bézard B, Encrenaz T, Griffin M (1997) External supply of oxygen to the atmospheres of the giant planets. Nature 389:159–162, DOI 10.1038/38236

Feuchtgruber H, Lellouch E, Orton G, de Graauw T, Vandenbussche B, Swinyard B, Moreno R, Jarchow C, Billebaud F, Cavalié T, Sidher S, Hartogh P (2013) The D/H ratio in the atmospheres of Uranus and Neptune from Herschel-PACS observations. Astron. Astrophys. 551:A126, DOI 10.1051/0004-6361/201220857

Fletcher LN, Orton GS, Teanby NA, Irwin PGJ (2009a) Phosphine on Jupiter and Saturn from Cassini/CIRS. Icarus 202:543–564, DOI 10.1016/j.icarus.2009.03.023

Fletcher LN, Orton GS, Teanby NA, Irwin PGJ, Bjoraker GL (2009b) Methane and its isotopologues on Saturn from Cassini/CIRS observations. Icarus 199:351–367, DOI 10.1016/j.icarus.2008.09.019

Fletcher LN, Drossart P, Burgdorf M, Orton GS, Encrenaz T (2010) Neptune's atmospheric composition from AKARI infrared spectroscopy. Astron. Astrophys. 514:A17, DOI 10.1051/0004-6361/200913358

Fletcher LN, Baines KH, Momary TW, Showman AP, Irwin PGJ, Orton GS, Roos-Serote M, Merlet C (2011) Saturn's tropospheric composition and clouds from Cassini/VIMS 4.6-5.1 μm nightside spectroscopy. Icarus 214(2):510–533, DOI 10.1016/j.icarus.2011.

06.006

Fletcher LN, Greathouse TK, Orton GS, Irwin PGJ, Mousis O, Sinclair JA, Giles RS (2014) The origin of nitrogen on Jupiter and Saturn from the 15N/14N ratio. Icarus 238:170–190, DOI 10.1016/j.icarus.2014.05.007

Fletcher LN, de Pater I, Orton GS, Hofstadter MD, Irwin PGJ, Roman MT, Toledo D (2020a) Ice Giant Circulation Patterns: Implications for Atmospheric Probes. Space Sci. Rev. 216(2):21, DOI 10.1007/s11214-020-00646-1

Fletcher LN, Kaspi Y, Guillot T, Showman AP (2020b) How Well Do We Understand the Belt/Zone Circulation of Giant Planet Atmospheres? Space Sci. Rev. 216(2):30, DOI 10.1007/s11214-019-0631-9

Fouchet T, Lellouch E, Bézard B, Encrenaz T, Drossart P, Feuchtgruber H, de Graauw T (2000a) ISO-SWS Observations of Jupiter: Measurement of the Ammonia Tropospheric Profile and of the ^{15}N/ ^{14}N Isotopic Ratio. Icarus 143(2):223–243, DOI 10.1006/icar. 1999.6255

Fouchet T, Lellouch E, Bézard B, Feuchtgruber H, Drossart P, Encrenaz T (2000b) Jupiter's hydrocarbons observed with ISO-SWS: vertical profiles of C_2H_6 and C_2H_2, detection of CH_3C_2H. Astron. Astrophys. 355:L13–L17

Fouchet T, Lellouch E, Cavalié T, Bézard B (2017) First determination of the tropospheric CO abundance in Saturn. In: AAS/Division for Planetary Sciences Meeting Abstracts #49, AAS/Division for Planetary Sciences Meeting Abstracts, p 209.05

Fouchet T, Greathouse T, Bézard B, Richter M, Moses J (2018a) First Measurements of Methyl Radical (CH_3) in Jupiter's atmosphere using TEXES/IRTF and EXES/SOFIA. In: AAS/Division for Planetary Sciences Meeting Abstracts, p 507.07

Fouchet T, Moreno R, Cavalié T, Lellouch E (2018b) Detection of HCN in Saturn's atmosphere, Central Bureau Electronic Telegram No. 4535

Frelikh R, Murray-Clay RA (2017) The Formation of Uranus and Neptune: Fine-tuning in Core Accretion. Astron. J. 154(3):98, DOI 10.3847/1538-3881/aa81c7

French RG, McGhee CA, Sicardy B (1998) Neptune's Stratospheric Winds from Three Central Flash Occultations. Icarus 136(1):27–49, DOI 10.1006/icar.1998.6001

Gardner JP, Mather JC, Clampin M, Doyon R, Greenhouse MA, Hammel HB, Hutchings JB, Jakobsen P, Lilly SJ, Long KS, Lunine JI, McCaughrean MJ, Mountain M, Nella J, Rieke GH, Rieke MJ, Rix HW, Smith EP, Sonneborn G, Stiavelli M, Stockman HS, Windhorst RA, Wright GS (2006) The James Webb Space Telescope. Space Sci. Rev. 123(4):485–606, DOI 10.1007/s11214-006-8315-7

Gautier D, Hersant F (2005) Formation and Composition of Planetesimals. Space Sci. Rev. 116:25–52, DOI 10.1007/s11214-005-1946-2

Gautier D, Conrath B, Flasar M, Hanel R, Kunde V, Chedin A, Scott N (1981) The helium abundance of Jupiter from Voyager. Journal of Geophysical Research 86(A10):8713–8720, DOI 10.1029/JA086iA10p08713

Gautier D, Hersant F, Mousis O, Lunine JI (2001) Enrichments in Volatiles in Jupiter: A New Interpretation of the Galileo Measurements. Astrophys. J. Lett. 550:L227–L230, DOI 10.1086/319648

Gierasch PJ, Conrath BJ (1985) Energy conversion processes in the outer planets. In: Hunt GE (ed) Recent Advances in Planetary Meteorology, pp 121–146

Giles RS, Fletcher LN, Irwin PGJ (2017) Latitudinal variability in Jupiter's tropospheric disequilibrium species: GeH_4, AsH_3 and PH_3. Icarus 289:254–269, DOI 10.1016/j.icarus. 2016.10.023

Gladstone GR, Yung YL (1983) An analysis of the reflection spectrum of Jupiter from 1500 A to 1740 A. Astrophys. J. 266:415–424, DOI 10.1086/160789

Grassi D, Adriani A, Mura A, Bolton S, Plainaki G C Sindoni, the JIRAM Juno team (2019) On the content of minor species in the upper Jupiter troposphere as inferred from JIRAM Juno data. In: EPSC Abstracts, vol 13, pp EPSC–DPS2019–239–1

Grevesse N, Asplund M, Sauval AJ, Scott P (2010) The chemical composition of the Sun. Astrophys. Space Sci. 328(1-2):179–183, DOI 10.1007/s10509-010-0288-z

Grevesse N, Scott P, Asplund M, Sauval AJ (2015) The elemental composition of the Sun. III. The heavy elements Cu to Th. Astron. Astrophys. 573:A27, DOI 10.1051/0004-6361/201424111

Guillot T (1995) Condensation of Methane, Ammonia, and Water and the Inhibition of Convection in Giant Planets. Science 269:1697–1699, DOI 10.1126/science.7569896

Guillot T (2005) The Interiors of Giant Planets: Models and Outstanding Questions. Annual Review of Earth and Planetary Sciences 33:493–530, DOI 10.1146/annurev.earth.32.101802.120325, astro-ph/0502068

Guillot T, Gautier D (2015) 10.16 - giant planets. In: Schubert G (ed) Treatise on Geophysics (Second Edition), second edition edn, Elsevier, Oxford, pp 529 – 557, DOI https://doi.org/10.1016/B978-0-444-53802-4.00176-7, URL http://www.sciencedirect.com/science/article/pii/B9780444538024001767

Guillot T, Hueso R (2006) The composition of Jupiter: sign of a (relatively) late formation in a chemically evolved protosolar disc. Mon. Not. R. Astron. Soc. 367(1):L47–L51, DOI 10.1111/j.1745-3933.2006.00137.x

Guillot T, Stevenson DJ, Li C, Atreya S, Ingersoll A, S B (2019) Storms and the distribution of ammonia in Jupiter's atmosphere. In: EPSC Abstracts, vol 13, pp EPSC–DPS2019–1142–1

Hartogh P, Lellouch E, Moreno R, Bockelée-Morvan D, Biver N, Cassidy T, Rengel M, Jarchow C, Cavalié T, Crovisier J, Helmich FP, Kidger M (2011) Direct detection of the Enceladus water torus with Herschel. Astron. Astrophys. 532:L2, DOI 10.1051/0004-6361/201117377

Helled R, Bodenheimer P (2014) The Formation of Uranus and Neptune: Challenges and Implications for Intermediate-mass Exoplanets. Astrophys. J. 789(1):69, DOI 10.1088/0004-637X/789/1/69

Helled R, Guillot T (2013) Interior Models of Saturn: Including the Uncertainties in Shape and Rotation. Astrophys. J. 767(2):113, DOI 10.1088/0004-637X/767/2/113

Helled R, Guillot T (2018) Internal Structure of Giant and Icy Planets: Importance of Heavy Elements and Mixing, Springer International Publishing AG, part of Springer Nature, p 44. DOI 10.1007/978-3-319-55333-7_44

Helled R, Lunine J (2014) Measuring Jupiter's water abundance by Juno: the link between interior and formation models. Mon. Not. R. Astron. Soc. 441:2273–2279, DOI 10.1093/mnras/stu516

Helled R, Anderson JD, Schubert G (2010) Uranus and Neptune: Shape and rotation. Icarus 210(1):446–454, DOI 10.1016/j.icarus.2010.06.037

Helled R, Anderson JD, Podolak M, Schubert G (2011) Interior Models of Uranus and Neptune. Astrophys. J. 726:15, DOI 10.1088/0004-637X/726/1/15

Helled R, Bodenheimer P, Podolak M, Boley A, Meru F, Nayakshin S, Fortney JJ, Mayer L, Alibert Y, Boss AP (2014) Giant Planet Formation, Evolution, and Internal Structure. In: Beuther H, Klessen RS, Dullemond CP, Henning T (eds) Protostars and Planets VI, p 643, DOI 10.2458/azu_uapress_9780816531240-ch028

Helled R, Nettelmann N, Guillot T (2020) Uranus and Neptune: Origin, Evolution and Internal Structure. Space Sci. Rev. 216(3):38, DOI 10.1007/s11214-020-00660-3

Hersant F, Gautier D, Huré JM (2001) A Two-dimensional Model for the Primordial Nebula Constrained by D/H Measurements in the Solar System: Implications for the Formation of Giant Planets. Astrophys. J. 554:391–407, DOI 10.1086/321355

Hersant F, Gautier D, Lunine JI (2004) Enrichment in volatiles in the giant planets of the Solar System. Planet. Space Sci. 52:623–641, DOI 10.1016/j.pss.2003.12.011

Hersant F, Gautier D, Tobie G, Lunine JI (2008) Interpretation of the carbon abundance in Saturn measured by Cassini. Planet. Space Sci. 56:1103–1111, DOI 10.1016/j.pss.2008.02.007

Hubbard WB, Podolak M, Stevenson DJ (1995) The interior of Neptune. In: Neptune and Triton, pp 109–138

Hubickyj O, Bodenheimer P, Lissauer JJ (2005) Accretion of the gaseous envelope of Jupiter around a 5 10 Earth-mass core. Icarus 179(2):415–431, DOI 10.1016/j.icarus.2005.06.021

Hue V, Cavalié T, Dobrijevic M, Hersant F, Greathouse TK (2015) 2D photochemical modeling of Saturn's stratosphere. Part I: Seasonal variation of atmospheric composition without meridional transport. Icarus 257:163–184, DOI 10.1016/j.icarus.2015.04.001

Hue V, Greathouse TK, Cavalié T, Dobrijevic M, Hersant F (2016) 2D photochemical modeling of Saturn's stratosphere. Part II: Feedback between composition and temperature. Icarus 267:334–343, DOI 10.1016/j.icarus.2015.12.007

Hue V, Hersant F, Cavalié T, Dobrijevic M, Sinclair JA (2018) Photochemistry, mixing and transport in Jupiter's stratosphere constrained by Cassini. Icarus 307:106–123, DOI 10.1016/j.icarus.2018.02.018

Iess L, Folkner WM, Durante D, Parisi M, Kaspi Y, Galanti E, Guillot T, Hubbard WB, Stevenson DJ, Anderson JD, Buccino DR, Casajus LG, Milani A, Park R, Racioppa P, Serra D, Tortora P, Zannoni M, Cao H, Helled R, Lunine JI, Miguel Y, Militzer B, Wahl S, Connerney JEP, Levin SM, Bolton SJ (2018) Measurement of Jupiter's asymmetric gravity field. Nature 555(7695):220–222, DOI 10.1038/nature25776

Iess L, Militzer B, Kaspi Y, Nicholson P, Durante D, Racioppa P, Anabtawi A, Galanti E, Hubbard W, Mariani MJ, Tortora P, Wahl S, Zannoni M (2019) Measurement and implications of Saturn's gravity field and ring mass. Science 364(6445):aat2965, DOI 10.1126/science.aat2965

Irwin PGJ, Toledo D, Garland R, Teanby NA, Fletcher LN, Orton GA, Bézard B (2018) Detection of hydrogen sulfide above the clouds in Uranus's atmosphere. Nature Astronomy 2:420–427, DOI 10.1038/s41550-018-0432-1

Irwin PGJ, Toledo D, Braude AS, Bacon R, Weilbacher PM, Teanby NA, Fletcher LN, Orton GS (2019a) Latitudinal variation in the abundance of methane (CH_4) above the clouds in Neptune's atmosphere from VLT/MUSE Narrow Field Mode Observations. Icarus 331:69–82, DOI 10.1016/j.icarus.2019.05.011

Irwin PGJ, Toledo D, Garland R, Teanby NA, Fletcher LN, Orton GS, Bézard B (2019b) Probable detection of hydrogen sulphide (H_2S) in Neptune's atmosphere. Icarus 321:550–563, DOI 10.1016/j.icarus.2018.12.014

Jacobson RA (2009) The Orbits of the Neptunian Satellites and the Orientation of the Pole of Neptune. Astron. J. 137(5):4322–4329, DOI 10.1088/0004-6256/137/5/4322

Jacobson RA (2014) The Orbits of the Uranian Satellites and Rings, the Gravity Field of the Uranian System, and the Orientation of the Pole of Uranus. Astron. J. 148(5):76, DOI 10.1088/0004-6256/148/5/76

Jacobson RA, Antreasian PG, Bordi JJ, Criddle KE, Ionasescu R, Jones JB, Mackenzie RA, Meek MC, Parcher D, Pelletier FJ, Owen J W M, Roth DC, Roundhill IM, Stauch JR (2006) The Gravity Field of the Saturnian System from Satellite Observations and

Spacecraft Tracking Data. Astron. J. 132(6):2520–2526, DOI 10.1086/508812

Janssen MA, Hofstadter MD, Gulkis S, Ingersoll AP, Allison M, Bolton SJ, Levin SM, Kamp LW (2005) Microwave remote sensing of Jupiter's atmosphere from an orbiting spacecraft. Icarus 173(2):447–453, DOI 10.1016/j.icarus.2004.08.012

Janssen MA, Ingersoll AP, Allison MD, Gulkis S, Laraia AL, Baines KH, Edgington SG, Anderson YZ, Kelleher K, Oyafuso FA (2013) Saturn's thermal emission at 2.2-cm wavelength as imaged by the Cassini RADAR radiometer. Icarus 226(1):522–535, DOI 10.1016/j.icarus.2013.06.008

Karkoschka E, Tomasko M (2009) The haze and methane distributions on Uranus from HST-STIS spectroscopy. Icarus 202:287–309, DOI 10.1016/j.icarus.2009.02.010

Karkoschka E, Tomasko MG (2011) The haze and methane distributions on Neptune from HST-STIS spectroscopy. Icarus 211:780–797, DOI 10.1016/j.icarus.2010.08.013

Kaspi Y, Showman AP, Hubbard WB, Aharonson O, Helled R (2013) Atmospheric confinement of jet streams on Uranus and Neptune. Nature 497(7449):344–347, DOI 10.1038/nature12131

Kaspi Y, Galanti E, Hubbard WB, Stevenson DJ, Bolton SJ, Iess L, Guillot T, Bloxham J, Connerney JEP, Cao H, Durante D, Folkner WM, Helled R, Ingersoll AP, Levin SM, Lunine JI, Miguel Y, Militzer B, Parisi M, Wahl SM (2018) Jupiter's atmospheric jet streams extend thousands of kilometres deep. Nature 555(7695):223–226, DOI 10.1038/nature25793

Knacke RF, Kim SJ, Ridgway ST, Tokunaga AT (1982) The abundances of CH4, CH3D, NH3, and PH3 in the troposphere of Jupiter derived from high-resolution 1100-1200/cm spectra. Astrophys. J. 262:388–395, DOI 10.1086/160432

Koskinen TT, Guerlet S (2018) Atmospheric structure and helium abundance on Saturn from Cassini/UVIS and CIRS observations. Icarus 307:161–171, DOI 10.1016/j.icarus.2018.02.020

Lambrechts M, Johansen A (2014) Forming the cores of giant planets from the radial pebble flux in protoplanetary discs. Astron. Astrophys. 572:A107, DOI 10.1051/0004-6361/201424343

Landgraf M, Liou JC, Zook HA, Grün E (2002) Origins of Solar System Dust beyond Jupiter. Astron. J. 123:2857–2861, DOI 10.1086/339704

Laraia AL, Ingersoll AP, Janssen MA, Gulkis S, Oyafuso F, Allison M (2013) Analysis of Saturn's thermal emission at 2.2-cm wavelength: Spatial distribution of ammonia vapor. Icarus 226:641–654, DOI 10.1016/j.icarus.2013.06.017

Leconte J, Selsis F, Hersant F, Guillot T (2017) Condensation-inhibited convection in hydrogen-rich atmospheres . Stability against double-diffusive processes and thermal profiles for Jupiter, Saturn, Uranus, and Neptune. Astron. Astrophys. 598:A98, DOI 10.1051/0004-6361/201629140

Leisawitz D, Amatucci E, Carter R, DiPirro M, Flores A, Staguhn J, Wu C, Allen L, Arenberg J, Armus L, Battersby C, Bauer J, Bell R, Beltran P, Benford D, Bergin E, Bradford CM, Bradley D, Burgarella D, Carey S, Chi D, Cooray A, Corsetti J, De Beck E, Denis K, Dewell L, East M, Edgington S, Ennico K, Fantano L, Feller G, Folta D, Fortney J, Generie J, Gerin M, Granger Z, Harpole G, Harvey K, Helmich F, Hilliard L, Howard J, Jacoby M, Jamil A, Kataria T, Knight S, Knollenberg P, Lightsey P, Lipscy S, Mamajek E, Martins G, Meixner M, Melnick G, Milam S, Mooney T, Moseley SH, Narayanan D, Neff S, Nguyen T, Nordt A, Olson J, Padgett D, Petach M, Petro S, Pohner J, Pontoppidan K, Pope A, Ramspacher D, Roellig T, Sakon I, Sandin C, Sandstrom K, Scott D, Sheth K, Steeves J, Stevenson K, Stokowski L, Stoneking E, Su K, Tajdaran K, Tompkins S, Vieira J, Webster C, Wiedner M, Wright EL, Zmuidzinas J (2018) The Origins Space Telescope:

mission concept overview. In: Proc. SPIE , Society of Photo-Optical Instrumentation Engineers (SPIE) Conference Series, vol 10698, p 1069815, DOI 10.1117/12.2313823

Lellouch E, Paubert G, Moreno R, Festou MC, Bezard B, Bockelee-Morvan D, Colom P, Crovisier J, Encrenaz T, Gautier D, Marten A, Despois D, Strobel DF, Sievers A (1995) Chemical and Thermal Response of Jupiter's Atmosphere Following the Impact of Comet Shoemaker-Levy-9. Nature 373:592–595, DOI 10.1038/373592a0

Lellouch E, Bézard B, Fouchet T, Feuchtgruber H, Encrenaz T, de Graauw T (2001) The deuterium abundance in Jupiter and Saturn from ISO-SWS observations. Astron. Astrophys. 370:610–622, DOI 10.1051/0004-6361:20010259

Lellouch E, Moreno R, Paubert G (2005) A dual origin for Neptune's carbon monoxide? Astron. Astrophys. 430:L37–L40, DOI 10.1051/0004-6361:200400127

Lellouch E, Bézard B, Strobel DF, Bjoraker GL, Flasar FM, Romani PN (2006) On the HCN and CO_2 abundance and distribution in Jupiter's stratosphere. Icarus 184:478–497, DOI 10.1016/j.icarus.2006.05.018

Lellouch E, Moreno R, Orton GS, Feuchtgruber H, Cavalié T, Moses JI, Hartogh P, Jarchow C, Sagawa H (2015) New constraints on the CH_4 vertical profile in Uranus and Neptune from Herschel observations. Astron. Astrophys. 579:A121, DOI 10.1051/0004-6361/201526518

Li C, Ingersoll A, Janssen M, Levin S, Bolton S, Adumitroaie V, Allison M, Arballo J, Bellotti A, Brown S, Ewald S, Jewell L, Misra S, Orton G, Oyafuso F, Steffes P, Williamson R (2017) The distribution of ammonia on Jupiter from a preliminary inversion of Juno microwave radiometer data. Geophys. Res. Lett. 44(11):5317–5325, DOI 10.1002/2017GL073159

Li C, Ingersoll A, Bolton S, Levin S, Janssen M, Atreya S, Lunine J, Steffes P, Brown S, Guillot T, Allison M, Arballo J, Bellotti A, Adumitroaie V, Gulkis S, Hodges A, Li L, Misra S, Orton G, Oyafuso F, Santos-Costa D, Waite H, Zhang Z (2020) The water abundance in Jupiter's equatorial zone. Nature Astronomy DOI 10.1038/s41550-020-1009-3

Lindal GF (1992) The Atmosphere of Neptune: an Analysis of Radio Occultation Data Acquired with Voyager 2. Astron. J. 103:967, DOI 10.1086/116119

Lindal GF, Wood GE, Levy GS, Anderson JD, Sweetnam DN, Hotz HB, Buckles BJ, Holmes DP, Doms PE, Eshleman VR, Tyler GL, Croft TA (1981) The atmosphere of Jupiter: an analysis of the Voyager radio occulation measurements. J. Geophys. Res. 86(A10):8721–8727, DOI 10.1029/JA086iA10p08721

Lindal GF, Sweetnam DN, Eshleman VR (1985) The atmosphere of Saturn - an analysis of the Voyager radio occultation measurements. Astron. J. 90:1136–1146, DOI 10.1086/113820

Lindal GF, Lyons JR, Sweetnam DN, Eshleman VR, Hinson DP (1987) The atmosphere of Uranus - Results of radio occultation measurements with Voyager 2. J. Geophys. Res. 92:14987–15001, DOI 10.1029/JA092iA13p14987

Lindal GF, Lyons JR, Sweetnam DN, Eshleman VR, Hinson DP (1990) The atmosphere of Neptune - Results of radio occultation measurements with the Voyager 2 spacecraft. Geophys. Res. Lett. 17:1733–1736, DOI 10.1029/GL017i010p01733

Lodders K (2004) Jupiter Formed with More Tar than Ice. Astrophys. J. 611:587–597, DOI 10.1086/421970

Lodders K (2010) Solar System Abundances of the Elements. Astrophysics and Space Science Proceedings 16:379, DOI 10.1007/978-3-642-10352-0_8

Lodders K, Fegley B Jr (1994) The origin of carbon monoxide in Neptunes's atmosphere. Icarus 112:368–375, DOI 10.1006/icar.1994.1190

Lunine JI, Stevenson DJ (1985) Thermodynamics of clathrate hydrate at low and high pressures with application to the outer solar system. Astrophys. J. Suppl. 58:493–531, DOI 10.1086/191050

Luszcz-Cook SH, de Pater I (2013) Constraining the origins of Neptune's carbon monoxide abundance with CARMA millimeter-wave observations. Icarus 222(1):379–400, DOI 10.1016/j.icarus.2012.11.002

Mahaffy PR, Niemann HB, Alpert A, Atreya SK, Demick J, Donahue TM, Harpold DN, Owen TC (2000) Noble gas abundance and isotope ratios in the atmosphere of Jupiter from the Galileo Probe Mass Spectrometer. J. Geophys. Res. 105:15061–15072, DOI 10.1029/1999JE001224

Marley MS, Gómez P, Podolak M (1995) Monte Carlo interior models for Uranus and Neptune. J. Geophys. Res. 100(E11):23349–23354, DOI 10.1029/95JE02362

Marten A, Gautier D, Owen T, Sanders DB, Matthews HE, Atreya SK, Tilanus RPJ, Deane JR (1993) First observations of CO and HCN on Neptune and Uranus at millimeter wavelengths and the implications for atmospheric chemistry. Astrophys. J. 406:285–297, DOI 10.1086/172440

Marten A, Matthews HE, Owen T, Moreno R, Hidayat T, Biraud Y (2005) Improved constraints on Neptune's atmosphere from submillimetre-wavelength observations. Astron. Astrophys. 429:1097–1105, DOI 10.1051/0004-6361:20041695

Matousek S (2007) The Juno New Frontiers mission. Acta Astronautica 61:932–939, DOI 10.1016/j.actaastro.2006.12.013

Mazevet S, Licari A, Chabrier G, Potekhin AY (2019) Ab initio based equation of state of dense water for planetary and exoplanetary modeling. Astron. Astrophys. 621:A128, DOI 10.1051/0004-6361/201833963

Meadows VS, Orton G, Line M, Liang MC, Yung YL, Van Cleve J, Burgdorf MJ (2008) First Spitzer observations of Neptune: Detection of new hydrocarbons. Icarus 197(2):585–589, DOI 10.1016/j.icarus.2008.05.023

Miguel Y, Guillot T, Fayon L (2016) Jupiter internal structure: the effect of different equations of state. Astron. Astrophys. 596:A114, DOI 10.1051/0004-6361/201629732

Militzer B, Hubbard WB (2013) Ab Initio Equation of State for Hydrogen-Helium Mixtures with Recalibration of the Giant-planet Mass-Radius Relation. Astrophys. J. 774(2):148, DOI 10.1088/0004-637X/774/2/148

Molter E, de Pater I, Sault RJ, Butler B, Luszcz-Cook S, Tollefson J, de Boer D (2019) Uranuss Tropospheric Circulation and Composition with ALMA and the VLA. In: EPSC Abstracts, vol 13, pp EPSC–DPS2019–726–1

Moreno R, Marten A, Lellouch E (2009) Search for PH$_3$ in the Atmospheres of Uranus and Neptune at Millimeter Wavelength. In: AAS/Division for Planetary Sciences Meeting Abstracts #41, AAS/Division for Planetary Sciences Meeting Abstracts, p 28.02

Moreno R, Lellouch E, Courtin R, Swinyard B, Fulton T, Orton G, Hartogh P, Jarchow C, Cavalié T, Feuchtgruber H, Team TH (2011) Observations of CO and HCN on Neptune with Herschel SPIRE. In: Geophysical Research Abstracts, Geophysical Research Abstracts, vol 13, pp EGU2011–8299

Moreno R, Lellouch E, Cavalié T, Moullet A (2017) Detection of CS in Neptune's atmosphere from ALMA observations. Astron. Astrophys. 608:L5, DOI 10.1051/0004-6361/201731472

Moses JI (2014) Chemical kinetics on extrasolar planets. Philosophical Transactions of the Royal Society of London Series A 372:20130073–20130073, DOI 10.1098/rsta.2013.0073

Moses JI, Poppe AR (2017) Dust ablation on the giant planets: Consequences for strato-
  spheric photochemistry. Icarus 297:33–58, DOI 10.1016/j.icarus.2017.06.002

Moses JI, Bézard B, Lellouch E, Gladstone GR, Feuchtgruber H, Allen M (2000a) Photo-
  chemistry of Saturn's Atmosphere. I. Hydrocarbon Chemistry and Comparisons with ISO
  Observations. Icarus 143(2):244–298, DOI 10.1006/icar.1999.6270

Moses JI, Lellouch E, Bézard B, Gladstone GR, Feuchtgruber H, Allen M (2000b) Pho-
  tochemistry of Saturn's Atmosphere. II. Effects of an Influx of External Oxygen. Icarus
  145:166–202, DOI 10.1006/icar.1999.6320

Moses JI, Fouchet T, Bézard B, Gladstone GR, Lellouch E, Feuchtgruber H (2005) Pho-
  tochemistry and diffusion in Jupiter's stratosphere: Constraints from ISO observations
  and comparisons with other giant planets. Journal of Geophysical Research (Planets)
  110:E08001, DOI 10.1029/2005JE002411

Moses JI, Visscher C, Fortney JJ, Showman AP, Lewis NK, Griffith CA, Klippenstein SJ,
  Shabram M, Friedson AJ, Marley MS, Freedman RS (2011) Disequilibrium Carbon, Oxy-
  gen, and Nitrogen Chemistry in the Atmospheres of HD 189733b and HD 209458b. As-
  trophys. J. 737:15, DOI 10.1088/0004-637X/737/1/15

Moses JI, Fletcher LN, Greathouse TK, Orton GS, Hue V (2018) Seasonal stratospheric
  photochemistry on Uranus and Neptune. Icarus 307:124–145, DOI 10.1016/j.icarus.2018.
  02.004

Mousis O, Alibert Y, Benz W (2006) Saturn's internal structure and carbon enrichment.
  Astron. Astrophys. 449(1):411–415, DOI 10.1051/0004-6361:20054224

Mousis O, Lunine JI, Madhusudhan N, Johnson TV (2012) Nebular Water Depletion as the
  Cause of Jupiter's Low Oxygen Abundance. Astrophys. J. Lett. 751:L7, DOI 10.1088/
  2041-8205/751/1/L7

Mousis O, Fletcher LN, Lebreton JP, Wurz P, Cavalié T, Coustenis A, Courtin R, Gautier D,
  Helled R, Irwin PGJ, Morse AD, Nettelmann N, Marty B, Rousselot P, Venot O, Atkinson
  DH, Waite JH, Reh KR, Simon AA, Atreya S, André N, Blanc M, Daglis IA, Fischer G,
  Geppert WD, Guillot T, Hedman MM, Hueso R, Lellouch E, Lunine JI, Murray CD,
  O'Donoghue J, Rengel M, Sánchez-Lavega A, Schmider FX, Spiga A, Spilker T, Petit
  JM, Tiscareno MS, Ali-Dib M, Altwegg K, Bolton SJ, Bouquet A, Briois C, Fouchet T,
  Guerlet S, Kostiuk T, Lebleu D, Moreno R, Orton GS, Poncy J (2014a) Scientific rationale
  for Saturn's in situ exploration. Planet. Space Sci. 104:29–47, DOI 10.1016/j.pss.2014.
  09.014

Mousis O, Lunine JI, Fletcher LN, Mandt KE, Ali-Dib M, Gautier D, Atreya S (2014b)
  New Insights on Saturn's Formation from its Nitrogen Isotopic Composition. Astrophys.
  J. Lett. 796(2):L28, DOI 10.1088/2041-8205/796/2/L28

Mousis O, Atkinson DH, Spilker T, Venkatapathy E, Poncy J, Frampton R, Coustenis A, Reh
  K, Lebreton JP, Fletcher LN, Hueso R, Amato MJ, Colaprete A, Ferri F, Stam D, Wurz
  P, Atreya S, Aslam S, Banfield DJ, Calcutt S, Fischer G, Holland A, Keller C, Kessler E,
  Leese M, Levacher P, Morse A, Muñoz O, Renard JB, Sheridan S, Schmider FX, Snik F,
  Waite JH, Bird M, Cavalié T, Deleuil M, Fortney J, Gautier D, Guillot T, Lunine JI, Marty
  B, Nixon C, Orton GS, Sánchez-Lavega A (2016) The Hera Saturn entry probe mission.
  Planet. Space Sci. 130:80–103, DOI 10.1016/j.pss.2015.06.020

Mousis O, Atkinson DH, Cavalié T, Fletcher LN, Amato MJ, Aslam S, Ferri F, Renard
  JB, Spilker T, Venkatapathy E, Wurz P, Aplin K, Coustenis A, Deleuil M, Dobrijevic M,
  Fouchet T, Guillot T, Hartogh P, Hewagama T, Hofstadter MD, Hue V, Hueso R, Lebreton
  JP, Lellouch E, Moses J, Orton GS, Pearl JC, Sánchez-Lavega A, Simon A, Venot O,
  Waite JH, Achterberg RK, Atreya S, Billebaud F, Blanc M, Borget F, Brugger B, Charnoz
  S, Chiavassa T, Cottini V, d'Hendecourt L, Danger G, Encrenaz T, Gorius NJP, Jorda L,

Marty B, Moreno R, Morse A, Nixon C, Reh K, Ronnet T, Schmider FX, Sheridan S, Sotin C, Vernazza P, Villanueva GL (2018) Scientific rationale for Uranus and Neptune in situ explorations. Planet. Space Sci. 155:12–40, DOI 10.1016/j.pss.2017.10.005

Mousis O, Ronnet T, Lunine JI (2019) Jupiter's Formation in the Vicinity of the Amorphous Ice Snowline. Astrophys. J. 875(1):9, DOI 10.3847/1538-4357/ab0a72

Mousis O, Atreya S, Lunine JI, Mandt KE, Marty B, Ronnet T (2020) Key atmospheric Signatures for identifying the source reservoirs of volatiles in Uranus and Neptune. Space Sci. Rev. this issue

Nettelmann N, Holst B, Kietzmann A, French M, Redmer R, Blaschke D (2008) Ab Initio Equation of State Data for Hydrogen, Helium, and Water and the Internal Structure of Jupiter. Astrophys. J. 683:1217–1228, DOI 10.1086/589806

Nettelmann N, Helled R, Fortney JJ, Redmer R (2013) New indication for a dichotomy in the interior structure of Uranus and Neptune from the application of modified shape and rotation data. Planet. Space Sci. 77:143–151, DOI 10.1016/j.pss.2012.06.019

Nettelmann N, Wang K, Fortney JJ, Hamel S, Yellamilli S, Bethkenhagen M, Redmer R (2016) Uranus evolution models with simple thermal boundary layers. Icarus 275:107–116, DOI 10.1016/j.icarus.2016.04.008

Niemann HB, Atreya SK, Carignan GR, Donahue TM, Haberman JA, Harpold DN, Hartle RE, Hunten DM, Kasprzak WT, Mahaffy PR, Owen TC, Way SH (1998) The composition of the Jovian atmosphere as determined by the Galileo probe mass spectrometer. J. Geophys. Res. 103:22831–22846, DOI 10.1029/98JE01050

Noll KS, Larson HP (1991) The spectrum of Saturn from 1990 to 2230 cm^{-1}: Abundances of AsH_3, CH_3D, CO, GeH_4, NH_3, and PH_3. Icarus 89(1):168–189, DOI 10.1016/0019-1035(91)90096-C

Noll KS, Knacke RF, Geballe TR, Tokunaga AT (1986) Detection of carbon monoxide in Saturn. Astrophys. J. Lett. 309:L91–L94, DOI 10.1086/184768

Norwood J, Hammel H, Milam S, Stansberry J, Lunine J, Chanover N, Hines D, Sonneborn G, Tiscareno M, Brown M, Ferruit P (2016a) Solar System Observations with the James Webb Space Telescope. Publ. Astron. Soc. Pac 128(2):025004, DOI 10.1088/1538-3873/128/960/025004

Norwood J, Moses J, Fletcher LN, Orton G, Irwin PGJ, Atreya S, Rages K, Cavalié T, Sánchez-Lavega A, Hueso R, Chanover N (2016b) Giant Planet Observations with the James Webb Space Telescope. Publ. Astron. Soc. Pac 128(1):018005, DOI 10.1088/1538-3873/128/959/018005

Öberg KI, Bergin EA (2016) Excess C/O and C/H in Outer Protoplanetary Disk Gas. Astrophys. J. Lett. 831(2):L19, DOI 10.3847/2041-8205/831/2/L19

Öberg KI, Murray-Clay R, Bergin EA (2011) The Effects of Snowlines on C/O in Planetary Atmospheres. Astrophys. J. Lett. 743(1):L16, DOI 10.1088/2041-8205/743/1/L16

Ollivier JL, Dobrijévic M, Parisot JP (2000) New photochemical model of Saturn's atmosphere. Planet. Space Sci. 48:699–716, DOI 10.1016/S0032-0633(00)00035-0

Orton GS, Fisher BM, Baines KH, Stewart ST, Friedson AJ, Ortiz JL, Marinova M, Ressler M, Dayal A, Hoffmann W, Hora J, Hinkley S, Krishnan V, Masanovic M, Tesic J, Tziolas A, Parija KC (1998) Characteristics of the Galileo probe entry site from Earth-based remote sensing observations. J. Geophys. Res. 103(E10):22791–22814, DOI 10.1029/98JE02380

Orton GS, Moses JI, Fletcher LN, Mainzer AK, Hines D, Hammel HB, Martin-Torres J, Burgdorf M, Merlet C, Line MR (2014) Mid-infrared spectroscopy of Uranus from the Spitzer infrared spectrometer: 2. Determination of the mean composition of the upper troposphere and stratosphere. Icarus 243:471–493, DOI 10.1016/j.icarus.2014.07.012

Owen T, Encrenaz T (2003) Element Abundances and Isotope Ratios in the Giant Planets and Titan. Space Sci. Rev. 106:121–138, DOI 10.1023/A:1024633603624

Owen T, Encrenaz T (2006) Compositional constraints on giant planet formation. Planet. Space Sci. 54:1188–1196, DOI 10.1016/j.pss.2006.05.030

Owen T, Mahaffy P, Niemann HB, Atreya S, Donahue T, Bar-Nun A, de Pater I (1999) A low-temperature origin for the planetesimals that formed Jupiter. Nature 402:269–270, DOI 10.1038/46232

Pearl JC, Conrath BJ (1991) The albedo, effective temperature, and energy balance of Neptune, as determined from Voyager data. J. Geophys. Res. 96:18921

Pearl JC, Conrath BJ, Hanel RA, Pirraglia JA (1990) The albedo, effective temperature, and energy balance of Uranus, as determined from Voyager IRIS data. Icarus 84:12–28, DOI 10.1016/0019-1035(90)90155-3

Perry ME, Waite Jr JH, Mitchell DG, Miller KE, Cravens TE, Perryman RS, Moore L, Yelle RV, Hsu HW, Hedman MM, Cuzzi JN, Strobel DF, Hamil OQ, Glein CR, Paxton LJ, Teolis BD, McNutt Jr RL (2018) Material flux from the rings of saturn into its atmosphere. Geophys. Res. Lett. 45(19):10,093–10,100, DOI 10.1029/2018GL078575, URL https://agupubs.onlinelibrary.wiley.com/doi/abs/10.1029/2018GL078575

Podolak M, Helled R (2012) What Do We Really Know about Uranus and Neptune? Astrophys. J. Lett. 759(2):L32, DOI 10.1088/2041-8205/759/2/L32

Podolak M, Hubbard WB, Stevenson DJ (1991) Models of Uranus' interior and magnetic field., pp 29–61

Pollack JB, Hubickyj O, Bodenheimer P, Lissauer JJ, Podolak M, Greenzweig Y (1996) Formation of the Giant Planets by Concurrent Accretion of Solids and Gas. Icarus 124:62–85, DOI 10.1006/icar.1996.0190

Prangé R, Fouchet T, Courtin R, Connerney JEP, McConnell JC (2006) Latitudinal variation of Saturn photochemistry deduced from spatially-resolved ultraviolet spectra. Icarus 180:379–392, DOI 10.1016/j.icarus.2005.11.005

Prinn RG, Barshay SS (1977) Carbon monoxide on Jupiter and implications for atmospheric convection. Science 198:1031–1034, DOI 10.1126/science.198.4321.1031

Redmer R, Mattsson TR, Nettelmann N, French M (2011) The phase diagram of water and the magnetic fields of Uranus and Neptune. Icarus 211(1):798–803, DOI 10.1016/j.icarus.2010.08.008

Roelfsema PR, Shibai H, Armus L, Arrazola D, Audard M, Audley MD, Bradford CM, Charles I, Dieleman P, Doi Y, Duband L, Eggens M, Evers J, Funaki I, Gao JR, Giard M, di Giorgio A, González Fernández LM, Griffin M, Helmich FP, Hijmering R, Huisman R, Ishihara D, Isobe N, Jackson B, Jacobs H, Jellema W, Kamp I, Kaneda H, Kawada M, Kemper F, Kerschbaum F, Khosropanah P, Kohno K, Kooijman PP, Krause O, van der Kuur J, Kwon J, Laauwen WM, de Lange G, Larsson B, van Loon D, Madden SC, Matsuhara H, Najarro F, Nakagawa T, Naylor D, Ogawa H, Onaka T, Oyabu S, Poglitsch A, Reveret V, Rodriguez L, Spinoglio L, Sakon I, Sato Y, Shinozaki K, Shipman R, Sugita H, Suzuki T, van der Tak FFS, Torres Redondo J, Wada T, Wang SY, Wafelbakker CK, van Weers H, Withington S, Vandenbussche B, Yamada T, Yamamura I (2018) SPICA- A Large Cryogenic Infrared Space Telescope: Unveiling the Obscured Universe. Publ. Astron. Soc. Aust. 35:e030, DOI 10.1017/pasa.2018.15

Röttgering H (2003) LOFAR, a new low frequency radio telescope. New Astron. Rev. 47(4-5):405–409, DOI 10.1016/S1387-6473(03)00057-5

Roulston MS, Stevenson DJ (1995) Prediction of neon depletion in jupiters atmosphere. Eos, Transactions American Geophysical Union 76:343

Safronov VS (1966) Sizes of the largest bodies falling onto the planets during their formation. Sov. Astron. 9:987–991

Scott P, Grevesse N, Asplund M, Sauval AJ, Lind K, Takeda Y, Collet R, Trampedach R, Hayek W (2015) The elemental composition of the Sun. I. The intermediate mass elements Na to Ca. Astron. Astrophys. 573:A25, DOI 10.1051/0004-6361/201424109

Seiff A, Kirk DB, Knight TCD, Young RE, Mihalov JD, Young LA, Milos FS, Schubert G, Blanchard RC, Atkinson D (1998) Thermal structure of Jupiter's atmosphere near the edge of a 5-μm hot spot in the north equatorial belt. J. Geophys. Res. 103:22857–22890, DOI 10.1029/98JE01766

Simon AA, Stern SA, Hofstadter M (2018) Outer Solar System Exploration: A Compelling and Unified Dual Mission Decadal Strategy for Exploring Uranus, Neptune, Triton, Dwarf Planets, and Small KBOs and Centaurs. arXiv e-prints arXiv:1807.08769

Simon AA, Fletcher LN, Arridge C, Atkinson D, Coustenis A, Ferri F, Hofstadter M, Masters A, Mousis O, Reh K, Turrini D, Witasse O (2020) A Review of the in Situ Probe Designs from Recent Ice Giant Mission Concept Studies. Space Sci. Rev. 216(1):17, DOI 10.1007/s11214-020-0639-1

Smith MD (1998) Estimation of a Length Scale to Use with the Quench Level Approximation for Obtaining Chemical Abundances. Icarus 132:176–184, DOI 10.1006/icar.1997.5886

Sromovsky LA, Fry PM (2008) The methane abundance and structure of Uranus' cloud bands inferred from spatially resolved 2006 Keck grism spectra. Icarus 193:252–266, DOI 10.1016/j.icarus.2007.08.037

Sromovsky LA, Fry PM, Kim JH (2011) Methane on Uranus: The case for a compact CH_4 cloud layer at low latitudes and a severe CH_4 depletion at high-latitudes based on re-analysis of Voyager occultation measurements and STIS spectroscopy. Icarus 215:292–312, DOI 10.1016/j.icarus.2011.06.024

Sromovsky LA, Karkoschka E, Fry PM, Hammel HB, de Pater I, Rages K (2014) Methane depletion in both polar regions of Uranus inferred from HST/STIS and Keck/NIRC2 observations. Icarus 238:137–155, DOI 10.1016/j.icarus.2014.05.016

Stanley S, Bloxham J (2004) Convective-region geometry as the cause of Uranus' and Neptune's unusual magnetic fields. Nature 428(6979):151–153, DOI 10.1038/nature02376

Stanley S, Bloxham J (2006) Numerical dynamo models of Uranus' and Neptune's magnetic fields. Icarus 184(2):556–572, DOI 10.1016/j.icarus.2006.05.005

Stone PH (1976) The meteorology of the Jovian atmosphere. In: Gehrels T (ed) IAU Colloq. 30: Jupiter: Studies of the Interior, Atmosp here, Magnetosphere and Satellites, pp 586–618

Teanby NA, Irwin PGJ (2013) An external origin for carbon monoxide on uranus from herschel/spire? Astrophys. J. Lett. 775(2):L49

Teanby NA, Irwin PGJ, Moses JI (2019) Neptune's carbon monoxide profile and phosphine upper limits from Herschel/SPIRE: Implications for interior structure and formation. Icarus 319:86–98, DOI 10.1016/j.icarus.2018.09.014

Thorngren D, Fortney JJ (2019) Connecting Giant Planet Atmosphere and Interior Modeling: Constraints on Atmospheric Metal Enrichment. Astrophys. J. Lett. 874(2):L31, DOI 10.3847/2041-8213/ab1137

Tollefson J, de Pater I, Luszcz-Cook S, DeBoer D (2019a) Neptune's Latitudinal Variations as Viewed with ALMA. Astron. J. 157(6):251, DOI 10.3847/1538-3881/ab1fdf

Tollefson J, de Pater I, Sault S, Butler B, Luszcz-Cook S, DeBoer D (2019b) Spatial variations on Neptune in the radio. In: EPSC Abstracts, pp EPSC–DPS2019–728–1

Tsai SM, Lyons JR, Grosheintz L, Rimmer PB, Kitzmann D, Heng K (2017) VULCAN: An Open-source, Validated Chemical Kinetics Python Code for Exoplanetary Atmospheres. Astrophys. J. Suppl. 228(2):20, DOI 10.3847/1538-4365/228/2/20

Valletta C, Helled R (2019) The Deposition of Heavy Elements in Giant Protoplanetary Atmospheres: The Importance of Planetesimal-Envelope Interactions. Astrophys. J. 871(1):127, DOI 10.3847/1538-4357/aaf427

Vazan A, Helled R (2020) Explaining the low luminosity of Uranus: a self-consistent thermal and structural evolution. Astron. Astrophys. 633:A50, DOI 10.1051/0004-6361/201936588

Venot O, Hébrard E, Agúndez M, Dobrijevic M, Selsis F, Hersant F, Iro N, Bounaceur R (2012) A chemical model for the atmosphere of hot Jupiters. Astron. Astrophys. 546:A43, DOI 10.1051/0004-6361/201219310

Venot O, Bounaceur R, Dobrijevic M, Hébrard E, Cavalié T, Tremblin P, Drummond B, Charnay B (2019) Reduced chemical scheme for modelling warm to hot hydrogen-dominated atmospheres. Astron. Astrophys. 624:A58, DOI 10.1051/0004-6361/201834861

Venot O, Cavalié T, Bounaceur R, Tremblin P, Brouillard L, Lhoussaine Ben Brahim R (2020) New chemical scheme for giant planet thermochemistry. Update of the methanol chemistry and new reduced chemical scheme. Astron. Astrophys. 634:A78, DOI 10.1051/0004-6361/201936697

Visscher C, Fegley B Jr (2005) Chemical Constraints on the Water and Total Oxygen Abundances in the Deep Atmosphere of Saturn. Astrophys. J. 623:1221–1227, DOI 10.1086/428493

Visscher C, Moses JI (2011) Quenching of Carbon Monoxide and Methane in the Atmospheres of Cool Brown Dwarfs and Hot Jupiters. Astrophys. J. 738:72, DOI 10.1088/0004-637X/738/1/72

Visscher C, Moses JI, Saslow SA (2010) The deep water abundance on Jupiter: New constraints from thermochemical kinetics and diffusion modeling. Icarus 209:602–615, DOI 10.1016/j.icarus.2010.03.029

von Zahn U, Hunten DM, Lehmacher G (1998) Helium in Jupiter's atmosphere: Results from the Galileo probe helium interferometer experiment. J. Geophys. Res. 103:22815–22830, DOI 10.1029/98JE00695

Vorburger A, Wurz P, Waite JH (2020) Chemical and isotopic composition measurements on atmospheric probes. Space Sci. Rev. this issue

Waite JH, Perryman RS, Perry ME, Miller KE, Bell J, Glein CR, Grimes J, Hedman M, Cuzzi J, Brockwell T, Teolis B, Moore L, Mitchell DG, Persoon A, Kurth WS, Wahlund JE, Morooka M, Hadid LZ, Walker J, Nagy A, Yelle R, Ledvina S, Johnson R, Tseng W, Tucker OJ, Ip WH (2018) Chemical interactions between Saturn's atmosphere and its rings. Science 362:51–

Wang D, Gierasch PJ, Lunine JI, Mousis O (2015) New insights on Jupiter's deep water abundance from disequilibrium species. Icarus 250:154–164, DOI 10.1016/j.icarus.2014.11.026

Wang D, Lunine JI, Mousis O (2016) Modeling the disequilibrium species for Jupiter and Saturn: Implications for Juno and Saturn entry probe. Icarus 276:21–38, DOI 10.1016/j.icarus.2016.04.027

Wilson HF, Militzer B (2010) Sequestration of Noble Gases in Giant Planet Interiors. Phys. Rev. Lett. 104(12):121101, DOI 10.1103/PhysRevLett.104.121101

Wong MH, Mahaffy PR, Atreya SK, Niemann HB, Owen TC (2004) Updated Galileo probe mass spectrometer measurements of carbon, oxygen, nitrogen, and sulfur on Jupiter.

Icarus 171:153–170, DOI 10.1016/j.icarus.2004.04.010

Wurz P, Abplanalp D, Tulej M, Lammer H (2012) A neutral gas mass spectrometer for the investigation of lunar volatiles. Planet. Space Sci. 74(1):264–269, DOI 10.1016/j.pss.2012.05.016

Yung YL, Drew WA, Pinto JP, Friedl RR (1988) Estimation of the reaction rate for the formation of CH3O from H + H2CO - Implications for chemistry in the solar system. Icarus 73:516–526, DOI 10.1016/0019-1035(88)90061-9